The Sustained Oscillation Modeling and Its Quantitative Suppression Methodology for GaN Devices

Jian Chen, *Student Member, IEEE*, Quanming Luo, *Member, IEEE*, Yuqi Wei, *Student Member, IEEE*, Xinyue Zhang, and Xiong Du, *Member, IEEE*

***Abstract*—Gallium nitride (GaN) devices are widely used due to their excellent performance when integrated into power electronics applications. However, owing to their low parasitic parameters and fast switching speed, they are more prone to instability than the silicon devices. The sustained oscillation discussed in this article is one of the instability problems, which may result in overshoot or even more serious device breakdown; thus, it is pretty necessary to suppress it effectively in practical applications. It is the first time to adopt an *RC* snubber to suppress the sustained oscillation in this article, which is very simple and cheap but effective. First, the sustained oscillation modeling based on a double pulse circuit is carried out. Then, the *RC* region is established quantitatively according to the root locus analysis results, which makes up for the defects of these qualitative methods before. Furthermore, it is first found that the sustained oscillation can be fully suppressed due to the existence of dipoles. Finally, the oscillation suppression effect within the *RC* region is compared with that outside the region by the simulation and experimental results, which are consistent with the theoretical analysis. Additionally, the possible negative influence of the added *RC* snubber is also discussed in this article, which shows that it has a little impact on the switching speed and energy loss, while the sustained oscillation is well suppressed.**

***Index Terms*—eGaN high electron mobility transistor (HEMTs), *RC* snubber, sustained oscillation.**

Manuscript received June 2, 2020; revised September 11, 2020 and November 6, 2020; accepted December 5, 2020. Date of publication December 9, 2020; date of current version March 5, 2021. This work was supported in part by the Nature Science Foundation Key Project of Chongqing in China under Grant cstc2019jcyj-zdxmX0005 and in part by the Shaanxi Provincial Key Laboratory of Industrial Automation under Grant SLGPT2019KF01-14. Recommended for publication by Associate Editor K. Sheng. *(Corresponding author: Quanming Luo.)*

Jian Chen, Xinyue Zhang, and Xiong Du are with the State Key Laboratory of Power Transmission Equipment and System Security and New Technology, School of Electrical Engineering, Chongqing University, Chongqing 400044, China (e-mail: 1746002496@qq.com; 20181113088t@cqu.edu.cn; duxiong@cqu.edu.cn).

Quanming Luo is with the State Key Laboratory of Power Transmission Equipment and System Security and New Technology, School of Electrical Engineering, Chongqing University, Chongqing 400044, China, and also with the School of Electrical Engineering, Shaanxi University of Technology, Hanzhong 723001, China (e-mail: lqm394@126.com).

Yuqi Wei is with the Department of Electrical Engineering, Chongqing University, Chongqing 400044, China, and also with the Department of Electrical Engineering, University of Arkansas, Fayetteville, AR 72701 USA (e-mail: yuqiwei@uark.edu).

This article has supplementary material provided by the authors and color versions of one or more figures available at https://doi.org/10.1109/TPEL.2020.3043472.

Digital Object Identifier 10.1109/TPEL.2020.3043472

I. Introduction

In recent years, the wide bandgap devices, such as gallium nitride (GaN) transistors, are being widely used as promising devices to achieve high-frequency, high-efficiency, and high-power-density power conversion due to a better figure of merit when compared with Si MOSFETs [1]–[6]. However, the merits of low parasitic parameters and fast switching speed may also cause instability problems for GaN-based power circuits, which may result in overvoltage, excessive electromagnetic interference, and even device breakdown [7], [9]. Specifically, the two main reasons are as follows [7]–[14]. On the one hand, the high change rate of the drain current produces a voltage across the common source inductor, which can cause a high gate–source voltage. On the other hand, the rapid change rate of the drain–source voltage produces a current in the gate–drain capacitor, and this current charges the gate–source capacitor, which can also cause a high gate–source voltage. To a certain extent, these two aspects act as a triggering mechanism leading to the onset of instability problems.

In [7], the divergence oscillation of the cascode GaN device under high-current turn-OFF condition has been studied. The capacitance mismatch between the GaN device and Si MOSFET may result in the oscillation. A simple solution is proposed by adding an additional capacitor in parallel with the Si MOSFET. In [13]–[15], the negative resistance theory and Barkhausen criterion are adopted to investigate the instability of SiC-based circuits, and some qualitative conclusions are given to suppress the occurrence of instability problems. For example, a small stray gate-loop inductance and high ON-resistance can reduce the risk of this instability. In addition, the false triggering oscillation (self-sustained oscillation) of the gate–source voltage in different devices is also studied in [16]–[22]. These studies consider various parasitic parameters and explore the effects of these parameters on the false triggering oscillation. It is found that reducing the gate inductance and common source inductance and increasing the gate resistance can suppress the false triggering oscillation to a certain extent. Besides the above problems, another instability problem is observed in the enhancement-mode GaN devices based half-bridge circuit [9]. The oscillation occurs when the active switch Q_2 is OFF and the inactive switch Q_1 conducts reversely, while the gate–source voltage v_{gs2} of Q_2 is normal, which means that Q_2 is normally turned OFF and v_{gs2}

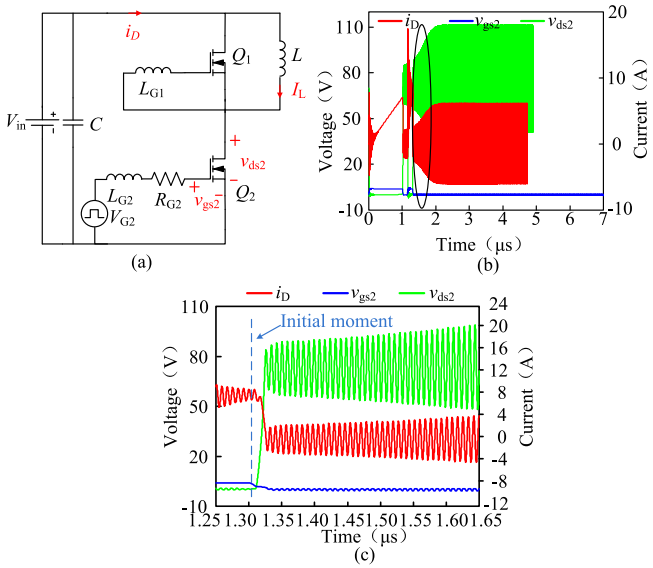

Fig. 1. Sustained oscillation of the half-bridge circuit. (a) GaN-based half-bridge circuit. (b) Sustained oscillation waveform. (c) Enlarged sustained oscillation waveform.

does not exceed the threshold voltage and cause false turn-ON, as shown in Fig. 1. Therefore, v_{gs2} is approximately clamped to 0 after Q_2 is turned OFF. In addition, it is noticeable that this oscillation phenomenon only occurs in GaN devices and does not occur in Si- or SiC-based circuits due to the unique reverse conduction characteristics of GaN devices. In [9], the influence of some parasitic parameters on this oscillation is explored and some suggestions are given to suppress this oscillation, such as reducing the common source inductance and increasing the gate resistance. However, these methods are qualitative and the suppression effects of them are quite limited. Accordingly, it is pretty necessary to find a quantitative method to solve the sustained oscillation problem to improve reliability in practical applications.

The *RC* snubber has been widely used to suppress the switching oscillations [23]–[30]. In [23] and [24], an *RC* snubber is adopted to suppress parasitic ringing in the circuit. However, the values of the *RC* parameters are given directly without explanation. Moreover, the theoretical analysis of their effect mechanism on parasitic ringing is not addressed, and only qualitative analysis is presented. In [25]–[29], some quantitative design methods for *RC* parameters are studied. However, the *RC* parameters are decided individually based on the designer's experience [25]–[27], which may not guarantee a sufficient level of ringing suppression. In [25] and [26], a second-order design method is proposed to roughly estimate the *RC* parameters, and the *RC* parameters are finally fixed by the experimental results. Obviously, this design method does not provide the adequate guidance for the quantitative design of *RC* parameters. An analytical technique for designing the *RC* snubber for the half-bridge configuration and the flyback converter is proposed in [28] and [29], respectively. Different from the article presented in [25] and [26], they use the root locus method to realize the quantitative design of the *RC* parameters of the third-order circuit, which achieved a better ringing suppression effect than the second-order design method in [25] and [26]. However, these quantitative methods for the *RC* design can only be applied to second-order or third-order circuits. In [30], the *RC* snubber is employed to suppress the false triggering oscillation of v_{gs2} by adding it across the gate–source terminal of the switch. Although the oscillation is not fully suppressed, the effect is satisfactory, and the *RC* design method can provide some guidance for high-order systems. However, since the sustained oscillation of v_{ds2} only occurs in GaN devices, it is doubtful whether the *RC* snubber can be used to suppress this oscillation satisfactorily or not due to the different oscillation mechanism between them. In addition, due to the different models of them, the design method in [30] is not completely applicable.

In this article, the *RC* snubber is first attempted to suppress the sustained oscillation by adding it across the drain–source terminal of the switch in a double pulse circuit, and the *RC* regions are determined quantitatively with full or well suppression effects. In Section II, the high-frequency equivalent model, including the *RC* snubber, is established by considering all parasitic parameters, and then the voltage across the drain–source terminal in the s-domain is derived. According to the expression of the drain–source voltage, dipoles are found by analyzing the root locus; thus, it has the opportunity to adopt dipole elimination to achieve full suppression of the sustained oscillation. This method is instructive for high-order circuits to establish dipoles through circuit design to achieve oscillation suppression, and it can also stimulate ideas for how to analyze and improve the performance of high-order systems. And then, the *RC* regions are quantitatively determined in Section III. In Section IV, the theoretical analysis results are fully verified by simulations and experiments. In addition, the switching speed and the energy loss with or without the *RC* snubber are also compared in this section, which verify the advantages of the proposed method. The conclusion derived from this article is summarized in Section V.

II. Derivation and Setting of an Equivalent Circuit Model

The double pulse circuit is taken as an example to study the sustained instability problem, which includes all the parasitic parameters of the circuit and device, as shown in Fig. 2(a). Q_1 is the inactive device, Q_2 is the active device and also the device under test. The current commutation occurs after Q_2 is turned OFF. The load inductor current I_L flows through Q_1 from its source to the drain, which may cause the gate–drain voltage v_{gd} to exceed the threshold voltage. Thus, the electrons are attracted to the heterostructure interface of the aluminum gallium nitride (AlGaN) and GaN so that the 2-D electron gas is reestablished, and the GaN devices conduct reverse current [31], [32]. At this time, Q_1 operates in the active region. During this process, the sustained oscillation may occur due to the parasitic parameters and reverse conduction characteristics of the GaN device.

In order to obtain the high-frequency equivalent circuit diagram of Fig. 2(a), the following assumptions are made.

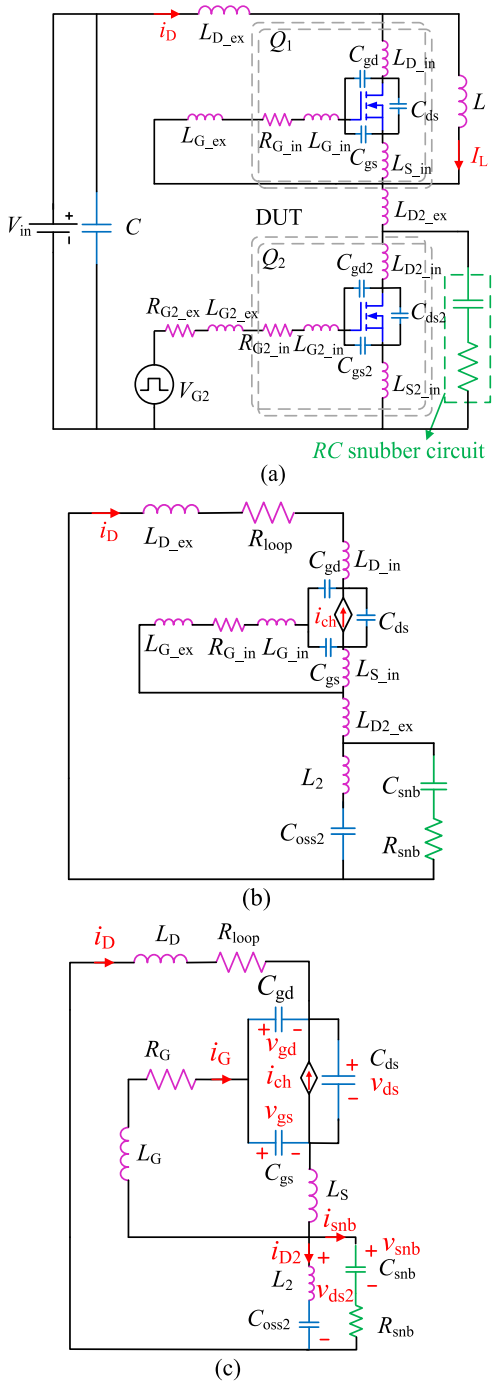

Fig. 2. (a) Schematic diagram of double pulse circuit with *RC* snubber circuit. (b) Simplified equivalent circuit. (c) Final high-frequency equivalent circuit.

1) Since the sustained oscillation occurs after Q_2 is turned OFF, and the gate–source voltage v_{gs2} of Q_2 is normal (v_{gs2} is approximately clamped to 0 after Q_2 is turned OFF), as shown in Fig. 1(c). Thus, the gate and source terminals of Q_2 are approximately shorted and only its output capacitor C_{oss2} is considered.
2) The decoupling capacitor C can be regarded as a shorted component due to its large capacitance, and its high-frequency impedance is sufficiently smaller than the other parameters.

TABLE I
DEFINITIONS OF THE SYMBOLS

Symbol	Description
V_{in}	Input voltage
L_D	Drain inductance, sum of L_{D_ex}, L_{D_in} and L_{D2_ex}
L	Inductance of load inductor
L_G	Gate inductance of Q_1, sum of L_{G_ex} and L_{G_in}
L_S	Common source inductance of Q_1, that is L_{S_in}
L_2	Parasitic inductance of Q_2, sum of L_{D2_in} and L_{S2_in}
C	Capacitance of decoupling capacitor
C_{ds}	Drain-source capacitance of Q_1
C_{gs}	Gate-source capacitance of Q_1
C_{gd}	Gate-drain capacitance of Q_1
C_{oss2}	Output capacitance of Q_2
C_{snb}	Capacitance of snubber capacitor
R_{loop}	Power loop resistance
R_G	Gate resistance of Q_1, that is R_{G_in}
R_{snb}	Resistance of snubber resistor
g_m	Reverse transconductance
i_D	Drain current of Q_1
i_G	Gate current of Q_1
i_{D2}	Output capacitance current of Q_2
i_{snb}	Current of snubber circuit
v_{ds}	Drain-source voltage of Q_1
v_{gs}	Gate-source voltage of Q_1
v_{gd}	Gate-drain voltage of Q_1
v_{gs2}	Gate-source voltage of Q_2
v_{ds2}	Drain-source voltage of Q_2
v_{snb}	Snubber capacitor voltage

3) The load inductor L can be regarded as an open component due to its large inductance, and its high-frequency impedance is sufficiently larger than the other parameters.
4) The inductor current charges the output capacitor of Q_1 reversely after Q_2 is turned OFF, which will cause an increase in v_{gd}, and Q_1 starts to conduct after v_{gd} exceeds its threshold voltage. Accordingly, Q_1 works in the active region and will have the channel current when the sustained oscillation of Q_2 occurs [9].

Based on these assumptions above, the simplified equivalent circuit is shown in Fig. 2(b). By integrating some components together, the final high-frequency equivalent circuit diagram is derived, as shown in Fig. 2(c), where L_D is the sum of the inductances L_{D_ex}, L_{D_in}, and L_{D2_ex}, the sum of L_{G_ex} and L_{G_in} is represented by L_G, L_2 is the sum of the inductances L_{D2_in} and L_{S2_in}, the parasitic gate resistance R_{G_in} and the common source inductance L_{S_in} are represented by R_G and L_S, respectively. The definitions of the main symbols used in this article are given in Table I.

From Fig. 2(c), the following equations are derived as:

$$0 = L_D\frac{di_D}{dt} + R_{loop}i_D + v_{ds} + L_S\frac{d(i_G+i_D)}{dt} + v_{ds2} \tag{1}$$

$$i_G = C_{gs}\frac{dv_{gs}}{dt} + C_{gd}\frac{dv_{gd}}{dt} = C_{iss}\frac{dv_{gs}}{dt} - C_{gd}\frac{dv_{ds}}{dt} \tag{2}$$

$$i_D = C_{ds}\frac{dv_{ds}}{dt} - C_{gd}\frac{dv_{gd}}{dt} - i_{ch} = C_{oss}\frac{dv_{ds}}{dt} - C_{gd}\frac{dv_{gs}}{dt} - i_{ch} \tag{3}$$

$$i_{ch} = g_m v_{gd} = g_m(v_{gs} - v_{ds}) \tag{4}$$

$$0 = L_G\frac{di_G}{dt} + i_G R_G + v_{\rm gs} + L_S\frac{d(i_G + i_D)}{dt} \tag{5}$$

$$v_{\rm ds2} = L_2\frac{di_{D2}}{dt} + v_{C\rm oss2} \tag{6}$$

$$i_{D2} = C_{\rm oss2}\frac{dv_{C\rm oss2}}{dt} \tag{7}$$

$$i_{\rm snb} = C_{\rm snb}\frac{dv_{\rm snb}}{dt} \tag{8}$$

$$v_{\rm ds2} = i_{\rm snb}R_{\rm snb} + v_{\rm snb} \tag{9}$$

$$i_D = i_{D2} + i_{\rm snb}. \tag{10}$$

The values of $R_{\rm snb}$ and $C_{\rm snb}$ are determined to suppress the sustained oscillation of $v_{\rm ds2}$; in the following, the s-domain equation of $v_{\rm ds2}$ is deduced out. The initial moment is shown in Fig. 1(c) after using the Laplace transform with the initial conditions $i_D(0) = i_{D2}(0) = I_0$, $i_G(0) = i_{\rm snb}(0) = 0$, $v_{\rm gs}(0) = 0$, $v_{\rm ds}(0) = V_0$, and $v_{\rm ds2}(0) = 0$, and the following equations are obtained as:

$$0 = (L_D + L_S)(si_D(s) - I_0) + R_{\rm loop}i_D(s) + v_{\rm ds}(s) + sL_S i_G(s) + v_{\rm ds2}(s) \tag{11}$$

$$i_G(s) = sC_{\rm iss}v_{\rm gs}(s) - C_{\rm gd}(sv_{\rm ds}(s) - V_0) \tag{12}$$

$$i_D(s) = C_{\rm oss}(sv_{\rm ds}(s) - V_0) - sC_{\rm gd}v_{\rm gs}(s) - g_m(v_{\rm gs}(s) - v_{\rm ds}(s)) \tag{13}$$

$$0 = sL_G i_G(s) + R_G i_G(s) + v_{\rm gs}(s) + sL_S i_G(s) + L_S(si_D(s) - I_0) \tag{14}$$

$$i_D(s) = \frac{sC_{\rm oss2}v_{\rm ds2}(s) + sC_{\rm oss2}L_2 I_0}{1 + s^2 C_{\rm oss2}L_2} + \frac{sC_{\rm snb}v_{\rm ds2}(s)}{sR_{\rm snb}C_{\rm snb} + 1} \tag{15}$$

where $i_D(s)$, $i_G(s)$, $v_{\rm gs}(s)$, $v_{\rm ds}(s)$, and $v_{\rm ds2}(s)$ are defined as the Laplace transforms of i_D, i_G, $v_{\rm gs}$, $v_{\rm ds}$, and $v_{\rm ds2}$, respectively.

From (11)–(15), the following expression of $v_{\rm ds2}$ is then derived as

$$v_{\rm ds2}(s) = \frac{N(s)}{M(s)} = \frac{a_0 s^5 + a_1 s^4 + a_2 s^3 + a_3 s^2 + a_4 s + a_5}{b_0 s^7 + b_1 s^6 + b_2 s^5 + b_3 s^4 + b_4 s^3 + b_5 s^2 + b_6 s + b_7} \tag{16}$$

where coefficients b_i ($i = 0, 1, 2, 3, 4, 5, 6, 7$) and a_j ($j = 0, 1, 2, 3, 4, 5$) can be derived through MATLAB, which is shown in the Appendix. From (16), it is clear that this is a seventh-order system.

III. Analysis and Design Methodology for *RC* Snubber to Suppress the Sustained Oscillation

In order to determine the *RC* values to suppress the sustained oscillation of $v_{\rm ds2}$ effectively, we need to study the characteristic equation $M(s) = 0$ of $v_{\rm ds2}(s)$. As can be seen from (16), $M(s)$ is a seventh-order polynomial. The sustained oscillation can be fully suppressed if the solutions of the characteristic equation, $M(s) = 0$, are all negative real numbers; then, $v_{\rm ds2}$ has no oscillation terms. When the solution of $M(s) = 0$ is a negative real number, the damping ratio is 1. However, it cannot guarantee that all solutions of the characteristic equations above third order are negative real numbers [28]–[30]. Based on this, all solutions of the characteristic equation $M(s) = 0$ above need to be explored. The values of some important parameters are given in Table II, which are obtained according to the parameters of our experimental prototype. Specifically, parasitic inductances that include device package inductances and printed circuit board (PCB) trace parasitic inductances are obtained through the LTspice model of the device and ANSYS Q3D extraction software, respectively. The transconductance and capacitances are obtained from the device datasheet [33]. It needs to be mentioned here that $R_{\rm loop}$ only contains dc resistance because the high-frequency ac resistance is much smaller than the dc resistance 0.2 Ω; thus, it can be ignored. After Q_2 is turned OFF, since the central tendency of the drain–source voltage of Q_2 is $V_{\rm in}$, the capacitances of Q_1 are obtained around $V_{\rm ds} = 0$ and the capacitance of Q_2 is approximately obtained at $V_{\rm in}$. The transconductance g_m is obtained around the threshold voltage. The specific method of obtaining capacitances and transconductance is shown in Fig. 3.

TABLE II
Key Circuit Parameters

Symbol	Value	Symbol	Value
$L_{\rm D}$	8.0 nH	$C_{\rm gd}$	0.06 nF
$L_{\rm G}$	5.2 nH	$C_{\rm oss2}$	0.19 nF
$L_{\rm S}$	0.2 nH	$R_{\rm G}$	1.3 Ω
L_2	0.4 nH	$R_{\rm loop}$	0.2 Ω
$C_{\rm iss}$	0.3 nF	$g_{\rm m}$	10 S
$C_{\rm oss}$	0.5 nF		

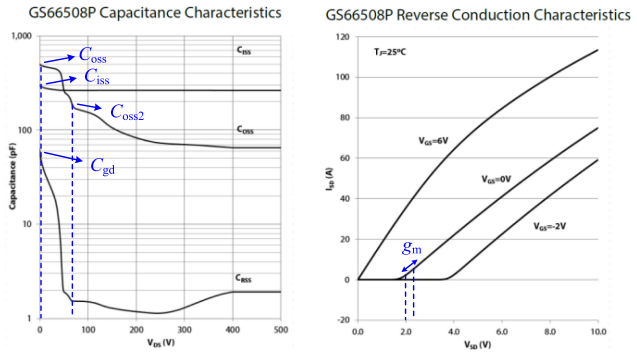

Fig. 3. (a) GS66508P capacitance characteristic diagram in the datasheet. (b) Reverse conduction characteristic of GS66508P.

When the *RC* snubber is not added, that is, $R_{\rm snb}$ and $C_{\rm snb}$ are equal to 0 so that $N(s)$ and $M(s)$ in (16) are fourth-order and fifth-order polynomials, respectively. Fig. 4 shows the pole-zero map of $v_{\rm ds2}(s)$ without the *RC* snubber. It can be observed that there are four zeros and five poles in Fig. 4(a). The five poles are a real pole p_1 and two pairs of complex conjugate poles p_2, $p_2{}^*$ and p_3, $p_3{}^*$. The real pole p_1 is negative and farther from the imaginary axis than p_2 and p_3; thus, it does not affect the stability of the system. It can be seen from Fig. 4(b) that p_3, $p_3{}^*$ are much closer to the imaginary axis than p_2, $p_2{}^*$; therefore, p_3,

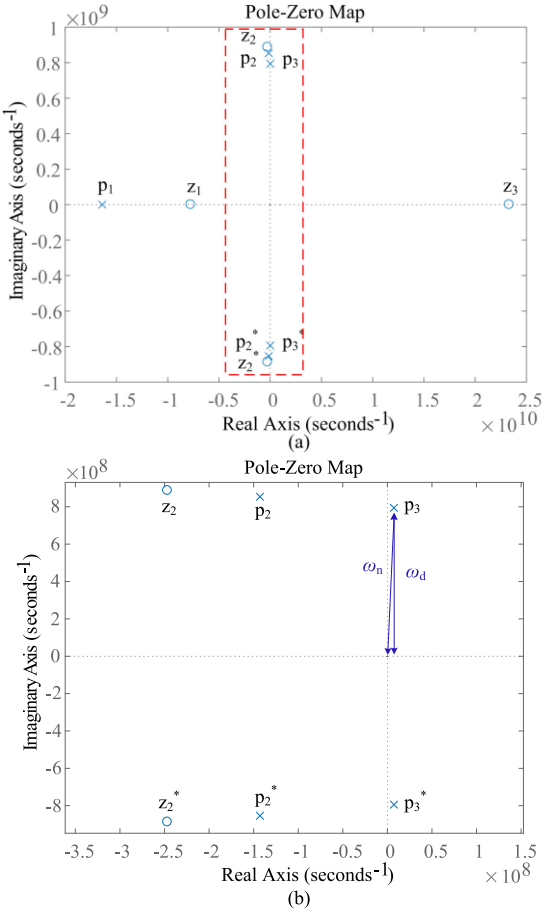

Fig. 4. Pole-zero map of $v_{ds2}(s)$ without the *RC* snubber circuit. (a) Pole-zero map of the $v_{ds2}(s)$. (b) Enlarged view.

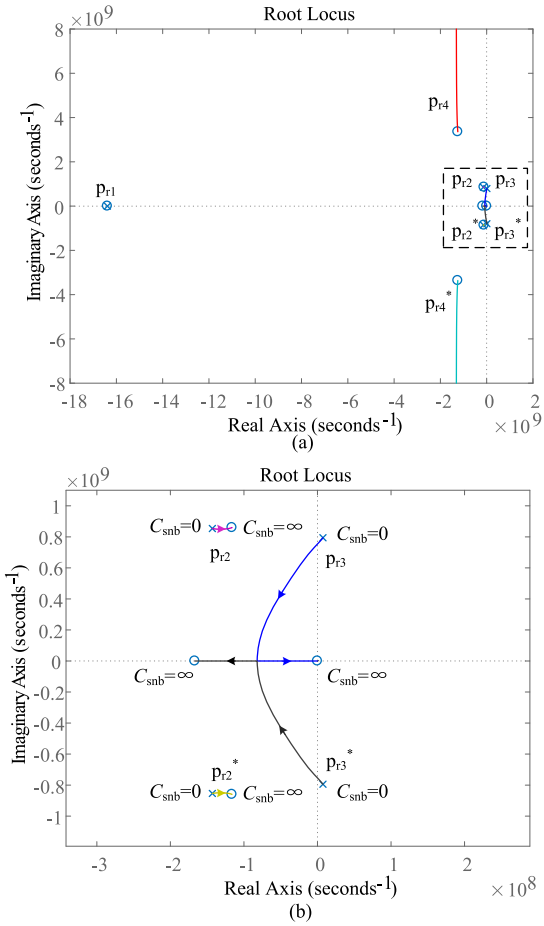

Fig. 5. (a) Root locus diagram of $M(s) = 0$ for parameter $C_{\rm snb}$ ($R_{\rm snb} = 1\ \Omega$). (b) Enlarged root locus diagram.

$p_3{}^*$ are the two dominant poles and they determine the stability of the system to a great extent.

The complex poles p_3, $p_3{}^*$ can be defined by their real and imaginary parts as

$$p_3, p_3* = \sigma \pm j\omega_d. \tag{17}$$

Hence, similar to the second-order system, the damping ratio ζ can be derived as (18) [34]. In addition, since the dominant pole p_3 is very close to the imaginary axis, the oscillation frequency can be approximately calculated, as shown in (19)

$$\zeta = \frac{-\sigma}{|P_3|} = \frac{-\sigma}{\sqrt{\sigma^2 + \omega_d^2}} = \frac{-\sigma}{\omega_n} \tag{18}$$

$$f_d \approx \frac{\omega_d}{2\pi}. \tag{19}$$

The damping ratio ζ can reflect the damping characteristic of $v_{ds2}(t)$. The larger the damping ratio ζ, the easier the oscillation is to be damped. Since $p_3, p_3{}^*$ are located in the right-half plane of $s, p_3, p_3{}^*$ have a positive real part, and ζ is less than 0. Therefore, the system is unstable, and the sustained oscillation of v_{ds2} will occur. If ζ>0 when the *RC* snubber is added, the poles have a negative real part and this sustained oscillation will disappear.

After the *RC* snubber is included, the characteristic equation $M(s) = 0$ is a seventh-order equation. As mentioned earlier, when all solutions of the characteristic equation are negative real numbers, the oscillation can be sufficiently suppressed. Therefore, it needs to study the root locus of all solutions of $M(s) = 0$. Considering $C_{\rm snb}$ as a variable and the equation $M(s) = 0$ can be transformed into the following form:

$$M_1 = 1 + \frac{C_{\rm snb} Q}{P} = 0. \tag{20}$$

The complete expression can be derived through MATLAB and the coefficients Q and P are shown in the Appendix.

By changing the value of the capacitance $C_{\rm snb}$ from zero to infinity, we can get the root locus of the characteristic equation. Fig. 5 shows the root locus of the characteristic equation $M(s) = 0$ when the *RC* snubber circuit is adopted ($R_{\rm snb} = 1\ \Omega$). It can be seen that after the *RC* snubber circuit is included, the root locus tends to the left-half plane of s. Therefore, the sustained oscillation tends to be suppressed. It can be seen from Fig. 5(a) that when $C_{\rm snb}$ changes from zero to infinity, the characteristic equation $M(s) = 0$ has a real solution with a damping ratio of 1 and three pairs of complex conjugate solutions. In practical applications, the effect on the system performance of the pole, which is three to six times farther away from the imaginary axis than the dominant pole, can often be ignored. In the process of $C_{\rm snb}$ changing from zero to infinity, $p_{\rm r1}$, $p_{\rm r4}$, and $p_{\rm r4}{}^*$ are always nondominant poles; thus, we can ignore their effects on

the system. In order to make this oscillation better suppressed, we only need to make the damping ratio of the other two pairs of complex conjugate solutions as large as possible. Fig. 5(b) is the enlarged view of the two pairs of complex conjugate solutions. As mentioned earlier, when all solutions of the characteristic equation $M(s) = 0$ are negative real numbers, the oscillation can be sufficiently suppressed. However, for this seventh-order equation, it is impossible to guarantee that all solutions of $M(s) = 0$ are real numbers according to Fig. 5(b).

When the snubber capacitance $C_{\rm snb}$ changes from zero to infinity, we can find that the poles p_{r2} and $p_{r2}{}^*$ will also become the dominant poles and their damping ratios are small, which may also affect the stability of the system. At the same time, it can also be seen that during the changing of $C_{\rm snb}$, the position of the poles p_{r2} and $p_{r2}{}^*$ changes very little. Therefore, it is valuable to try to eliminate these poles using the zero-point equation. To this end, the dipole elimination method based on the root locus analysis to determine the $R_{\rm snb}$ and $C_{\rm snb}$ value regions quantitatively is adopted in the following for this seventh-order system.

Similar to the method above, we can get the zero-point equation $N(s) = 0$ according to (16). Considering Csnb as a variable and transforming the equation into the following form:

$$N_1 = 1 + \frac{C_{\rm snb} Q_1}{P_1} = 0 \tag{21}$$

where the coefficients Q_1 and P_1 are also shown in the Appendix.

By changing the value of the capacitance $C_{\rm snb}$ from zero to infinity according to $C_{\rm snb}Q_1/P_1$, we can get the root locus of $N(s) = 0$. Fig. 6 shows the root locus diagram of $N(s) = 0$ when the snubber resistance $R_{\rm snb} = 1\ \Omega$. It can be seen that there are five zero points, including three real zeros and a pair of complex conjugate zeros. It is found that the position of the pair of complex conjugate zeros z_{r2} and $z_{r2}{}^*$ does not change according to Fig. 6(b). The enlarged root locus diagram of $M(s) = 0$ and $N(s) = 0$ is shown in Fig. 7. It can be seen that when $C_{\rm snb}$ changes from zero to infinity, the distances between the zero root loci of z_{r2}, $z_{r2}{}^*$ and the pole root loci of p_{r2}, $p_{r2}{}^*$ are approximately an order of magnitude smaller than their own modulus, which forms two pairs of dipoles. Therefore, the influence of the root loci of p_{r2} and $p_{r2}{}^*$ on the system performance is negligible. Accordingly, we only need the root loci of p_{r3} and $p_{r3}{}^*$ to have a larger damping ratio so that the oscillation is better suppressed. When the damping ratio is greater than 0.4, it will have well oscillation suppression effect [35]. Therefore, we attempt to take the damping ratio greater than 0.4 as the design standard, which will be verified by the test results in Section IV. According to Fig. 7, when $C_{\rm snb} > 3.35$ nF, the damping ratio of p_{r3} and $p_{r3}{}^*$ is greater than 0.4, and the oscillation can be well damped. When $C_{\rm snb} > 18.9$ nF, the damping ratio is the largest ($\zeta = 1$), and the sustained oscillation can be fully suppressed.

Similar to the analysis above, Fig. 8 shows the root locus diagram of the characteristic equation $M(s) = 0$ and $N(s) = 0$ when the snubber resistance $R_{\rm snb}$ changes from 0.5 to 4 Ω. It can be seen that p_{r1}, p_{r4}, and $p_{r4}{}^*$ are always nondominant poles, so we can ignore their effects. Fig. 8(b) shows the enlarged root locus diagram of $M(s) = 0$ and $N(s) = 0$. It can be seen

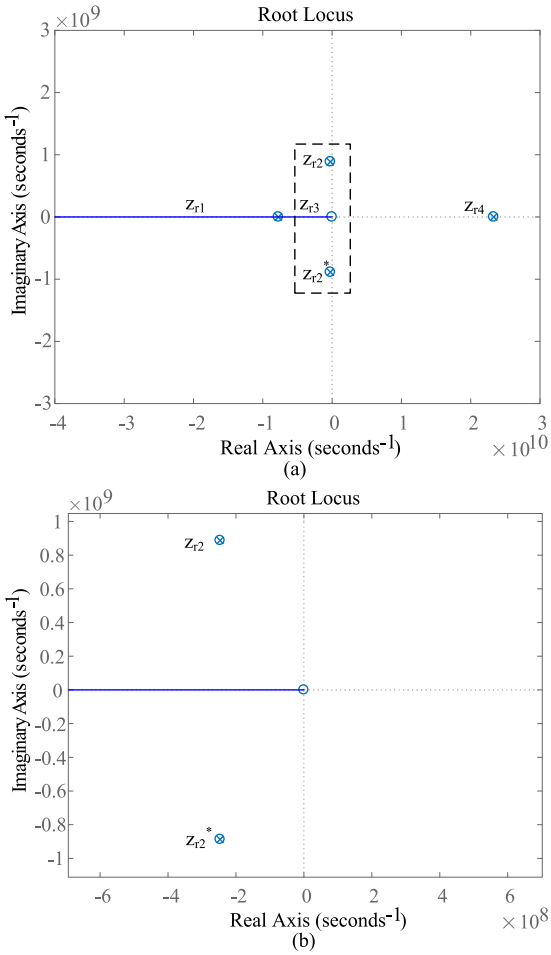

Fig. 6. (a) Root locus diagram of $N(s) = 0$ for parameter $C_{\rm snb}$ ($R_{\rm snb} = 1\ \Omega$). (b) Enlarged root locus diagram.

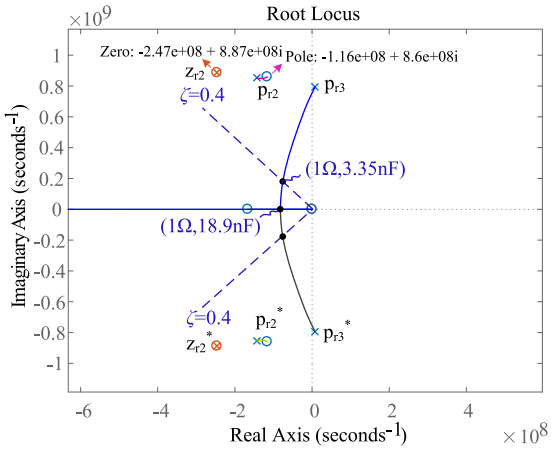

Fig. 7. Enlarged root locus diagram of $M(s) = 0$ and $N(s) = 0$ for parameter $C_{\rm snb}$ ($R_{\rm snb} = 1\ \Omega$).

that z_{r2}, $z_{r2}{}^*$ and $p_{\rm r2}$, $p_{\rm r2}{}^*$ still form dipoles in the process of $C_{\rm snb}$ changing from zero to infinity; thus, their impact on the system performance can be neglected. Therefore, we only need the root loci of p_{r3} and $p_{r3}{}^*$ to have a large damping ratio to make the oscillation well suppressed. For example, when the snubber resistance $R_{\rm snb} = 3\ \Omega$, if $C_{\rm snb} > 0.77$ nF, the damping

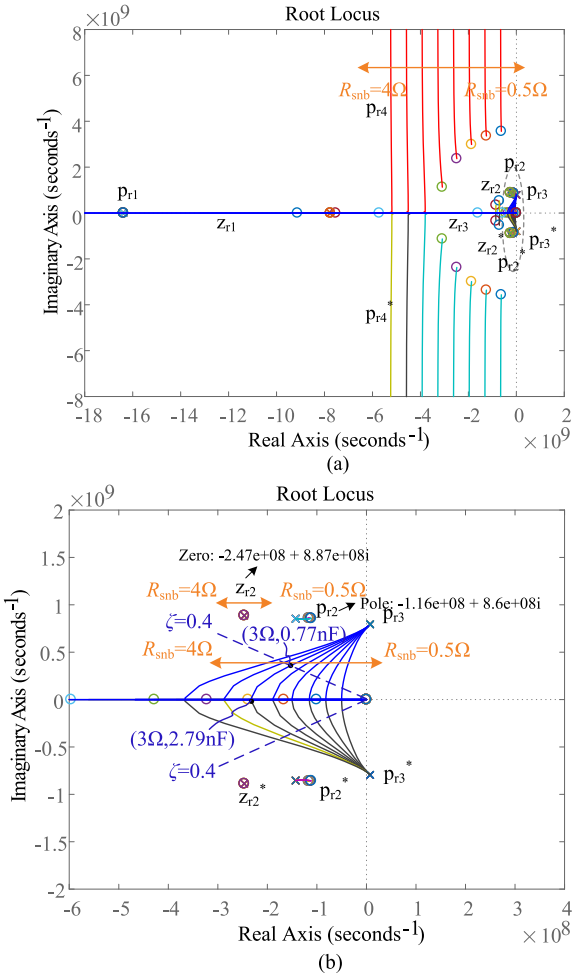

Fig. 8. (a) Root locus diagram of $M(s) = 0$ and $N(s) = 0$ for parameter C_{snb} (R_{snb} from 0.5 to 4 Ω). (b) Enlarged root locus diagram.

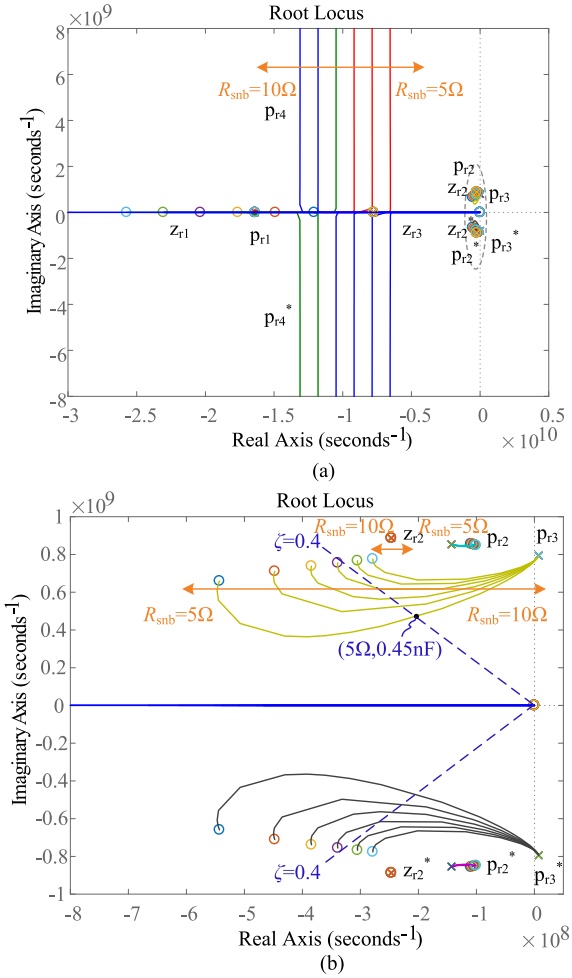

Fig. 9. (a) Root locus diagram of $M(s) = 0$ and $N(s) = 0$ for parameter C_{snb} (R_{snb} from 5 to 10 Ω). (b) Enlarged root locus diagram.

ratio of p_{r3} and $p_{r3}{}^*$ is greater than 0.4, and the oscillation can be well damped. When $C_{\mathrm{snb}} > 2.79$ nF, the damping ratio is the largest ($\zeta = 1$), and the sustained oscillation can be fully suppressed.

Fig. 9 shows the root locus diagram of the characteristic equation $M(s) = 0$ and $N(s) = 0$ when the snubber resistance R_{snb} changes from 5 to 10 Ω. It can be seen that no matter how C_{snb} changes, there are always two pairs of complex conjugate solutions p_{r2}, $p_{r2}{}^*$ and p_{r3}, $p_{r3}{}^*$. Fig. 9(b) shows the enlarged root locus diagram of $M(s) = 0$ and $N(s) = 0$. According to Fig. 9(b), z_{r2}, $z_{r2}{}^*$ and p_{r2}, $p_{r2}{}^*$ still form dipoles, and their influence on the system performance can still be ignored. However, the dominant poles p_{r3}, $p_{r3}{}^*$ always have oscillation terms, so the oscillation cannot be fully suppressed. When the snubber resistance $R_{\mathrm{snb}} = 5$ Ω, if $C_{\mathrm{snb}} > 0.45$ nF, the damping ratio of p_{r3} and $p_{r3}{}^*$ is greater than 0.4, and the oscillation can be well damped. When the snubber resistance $R_{\mathrm{snb}} = 10$ Ω, the damping ratio of dominant poles p_{r3} and $p_{r3}{}^*$ is always less than 0.4 in the process of C_{snb} changing from zero to infinity. Therefore, their suppression effect on the sustained oscillation is not well, and these design values should be excluded.

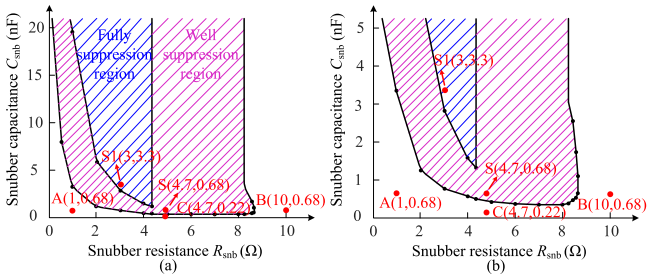

Fig. 10. (a) $R_{\mathrm{snb}} - C_{\mathrm{snb}}$ region where the sustained oscillation is considered to be fully or well suppressed. (b) Enlarged view when the range of C_{snb} is 0 to 5 nF.

According to the above analysis method, it can be concluded that when the snubber resistance $R_{\mathrm{snb}} = 1$ Ω, 3 Ω, and 5 Ω, the design regions of C_{snb} are $C_{\mathrm{snb}} > 3.35$ nF ($\zeta > 0.4$), $C_{\mathrm{snb}} > 18.9$ nF ($\zeta = 1$), $C_{\mathrm{snb}} > 0.77$ nF ($\zeta > 0.4$), $C_{\mathrm{snb}} > 2.79$ nF ($\zeta = 1$), and $C_{\mathrm{snb}} > 0.45$ nF ($\zeta > 0.4$), respectively. In addition, when the snubber resistance R_{snb} changes, such as $R_{\mathrm{snb}} = 2$ Ω and $R_{\mathrm{snb}} = 4$ Ω, the design regions of C_{snb} are $C_{\mathrm{snb}} > 1.28$ nF ($\zeta > 0.4$), $C_{\mathrm{snb}} > 5.93$ nF ($\zeta = 1$), $C_{\mathrm{snb}} > 0.56$ nF ($\zeta > 0.4$), and $C_{\mathrm{snb}} > 1.54$ nF ($\zeta = 1$), respectively. Using the same method, the final *RC* design region is obtained, as shown in Fig. 10(a). The *RC*

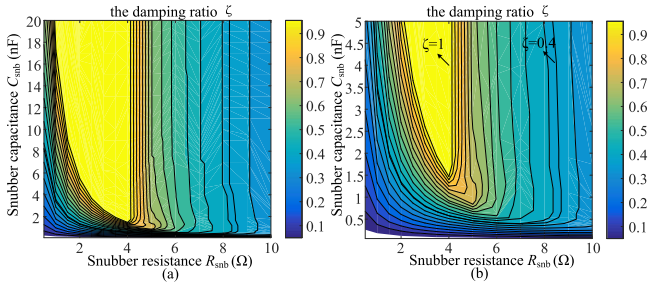

Fig. 11. (a) Relationship among snubber resistance $R_{\rm snb}$, snubber capacitance $C_{\rm snb}$, and damping ratio ζ. (b) Enlarged view when the range of $C_{\rm snb}$ is 0 to 5 nF.

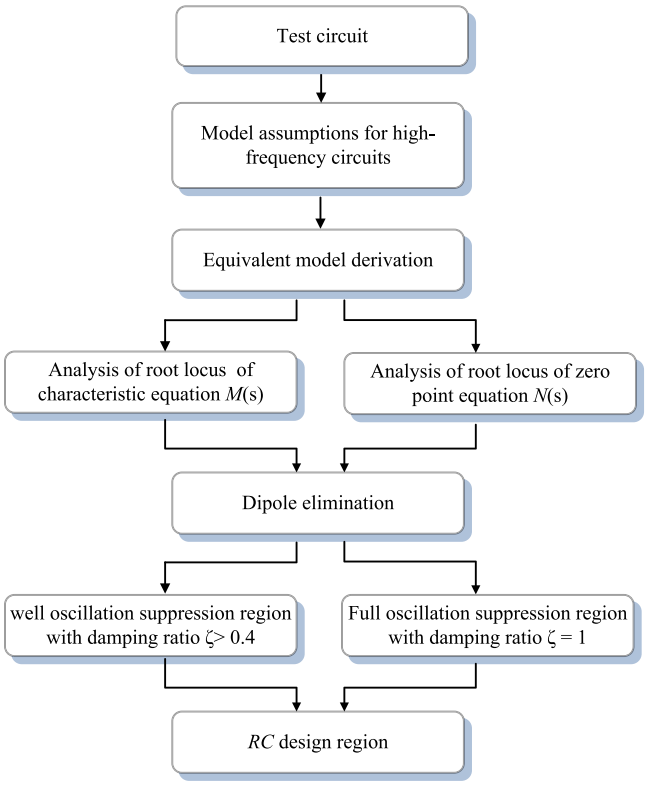

Fig. 12. Method for obtaining *RC* region.

values in the blue shaded region enable the sustained oscillation to be fully suppressed and the *RC* values in the purple shaded region enable the oscillation to be well suppressed. Fig. 11 shows the contour plot of snubber resistance, snubber capacitance, and damping ratio of dominant pole p_{r3}. It can be seen when $R_{\rm snb}$ is large, the damping ratio of dominant pole p_{r3} is always less than 0.4 in the process of $C_{\rm snb}$ changing from zero to infinity.

As described above, the method for obtaining the *RC* region can be summarized, as shown in Fig. 12. It is noticeable that the analysis of the equivalent equation is divided into two parts: drawing the pole root locus and the zero root locus. Once the dipole is formed between the zero and the pole, the effect of the pole on the system performance can be ignored. This method can stimulate an idea for how to analyze and improve the performance of high-order systems.

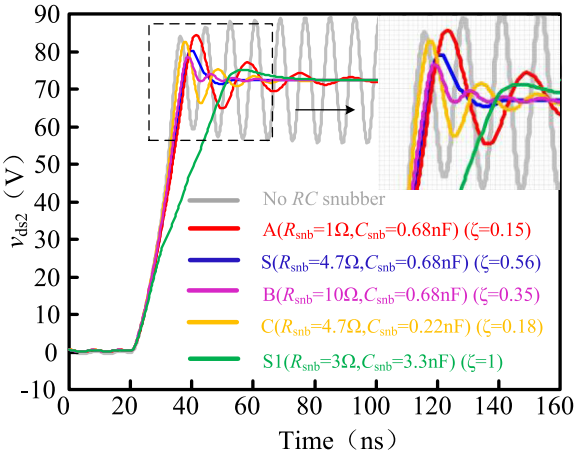

Fig. 13. Simulation comparison of the oscillation suppression effect (within the *RC* design region, outside the *RC* design region, and no *RC* snubber).

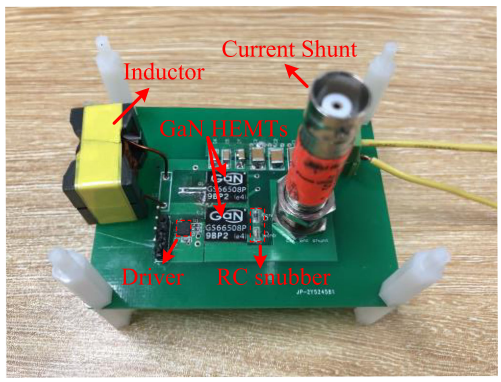

Fig. 14. Experimental configuration and prototype of a double pulse test circuit.

IV. Simulation and Experimental Verification

A. Simulation Verification

The simulation is performed to verify the above analysis through the Ltspice software. The simulation circuit is a double pulse circuit and all the device parasitic parameters are taken into account. Especially, the switching device is GS66508P using the manufacturer's LTspice model. The input voltage $V_{\rm in}$ is 70 V and the inductor current I_L is 8 A. In order to verify the oscillation suppression effect of the designed *RC* region, the oscillation suppression effect within the region is compared with that outside the region. In the designed *RC* region, we select point *S* (4.7 Ω, 0.68 nF) in the well suppressed region and point *S*1 (3 Ω, 3.3 nF) in the fully suppressed region to compare their oscillation suppression effect with these points locating outside the designed region. The selected values outside the region are shown in Fig. 10(b), which include points *A* (1 Ω, 0.68 nF), *B* (10 Ω, 0.68 nF), and *C* (4.7 Ω, 0.22 nF).

Fig. 13 shows the simulation result, which is a comparison of the oscillation suppression effect (within the designed *RC* region, outside the region, and no *RC* snubber). It can be seen that the sustained oscillation within the designed region (point *S* and point *S*1) can be well suppressed. However, for these points outside the *RC* design region (including points *A, B,* and *C*), the

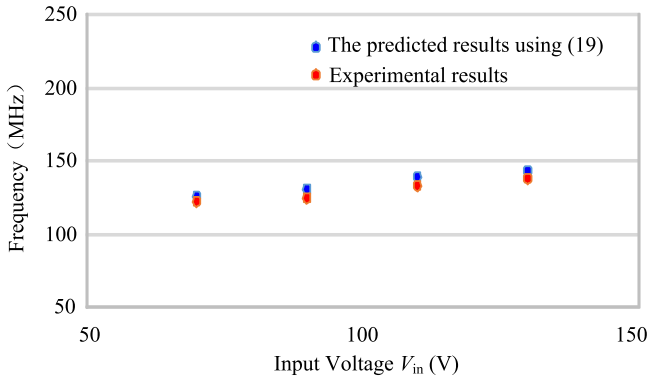

Fig. 15. Comparison of prediction frequency and experimental measurement frequency.

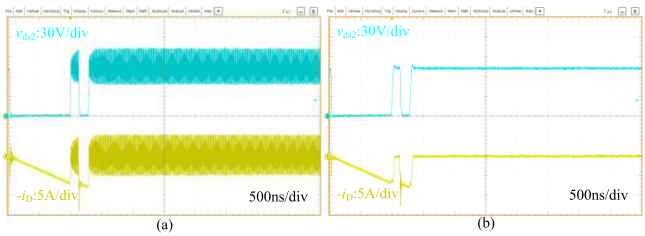

Fig. 16. Experimental results without *RC* snubber and with the *RC* snubber. (a) Without *RC* snubber. (b) With *RC* snubber.

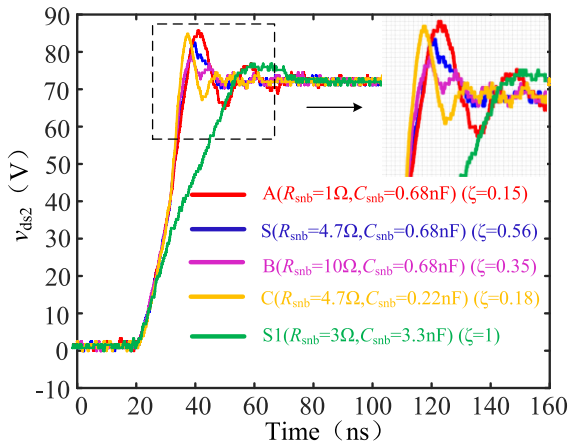

Fig. 17. Experimental results' comparison of the oscillation suppression effect within the *RC* design region and outside the *RC* design region.

suppression effects of the sustained oscillation are not as good as those within the *RC* design region.

B. Experimental Verification

Fig. 14 shows the experimental prototype of the double pulse test circuit. The input voltage of the experiment is 70 V and the inductor current is 8 A, which is consistent with the simulation conditions. Its specifications and circuit parameters are the same as those given in Table II. Specifically, the switching device is GS66508P, and the driver is the LM5114. The current shunt is SSDN-10, which has a high bandwidth (2000 MHz) and the accurate resistance (0. 1 Ω).

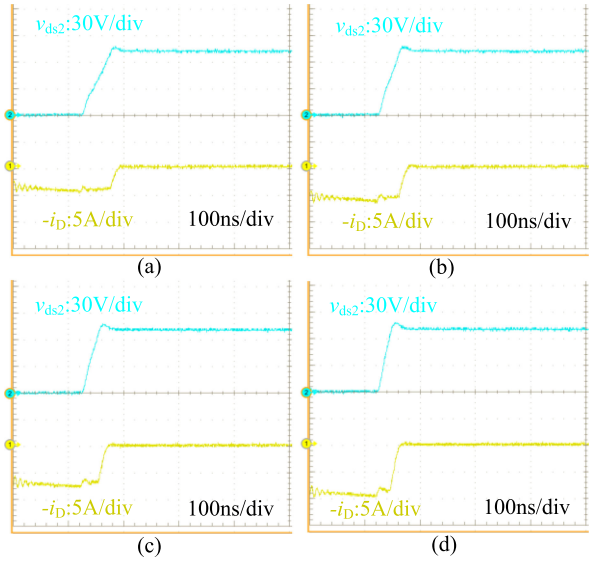

Fig. 18. Oscillation suppression effect for the proposed *RC* design method (point *S*1) under different inductor currents. (a) $I_L = 4$ A. (b) $I_L = 6$ A. (c) $I_L = 8$ A. (d) $I_L = 10$ A.

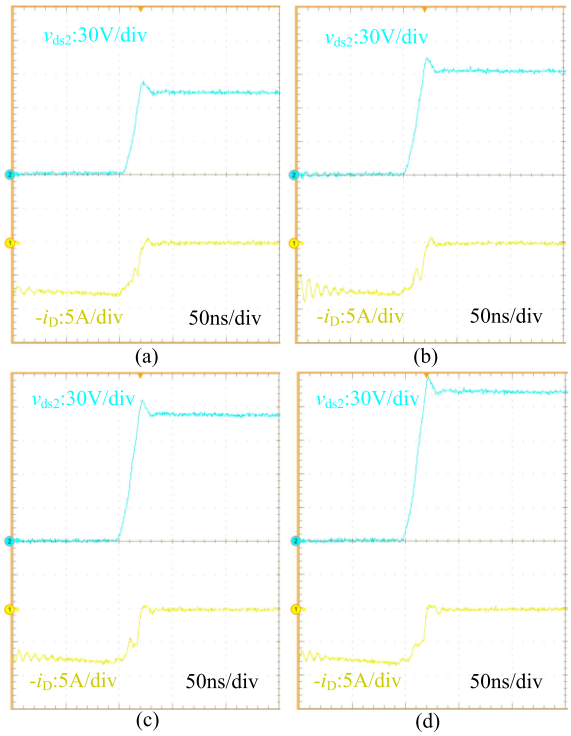

Fig. 19. Oscillation suppression effect for the proposed *RC* design method (point *S*) under different input voltages ($I_L = 8$ A). (a) $V_{in} = 70$ V. (b) $V_{in} = 90$ V. (c) $V_{in} = 110$ V. (d) $V_{in} = 130$ V.

In order to verify the accuracy of the proposed model, when no *RC* is added, the sustained oscillation frequency predicted by (19) is compared with the experimental results, as shown in Fig. 15. It can be seen that when the input voltage changes, the experimentally measured oscillation frequency is in good agreement with the predicted oscillation frequency. Therefore, the proposed model has good accuracy.

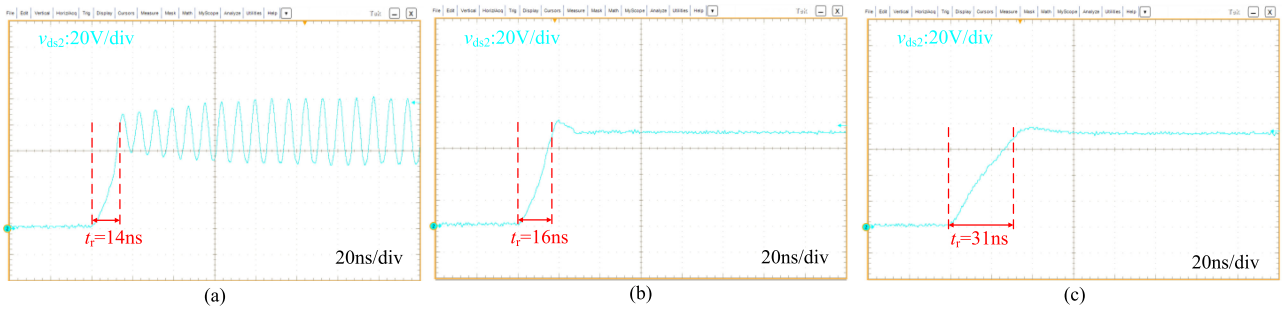

Fig. 20. Switching speed without *RC* and with *RC* snubber circuit. (a) Without *RC* snubber. (b) With *RC* snubber (point *S*). (c) With *RC* snubber (point *S*1).

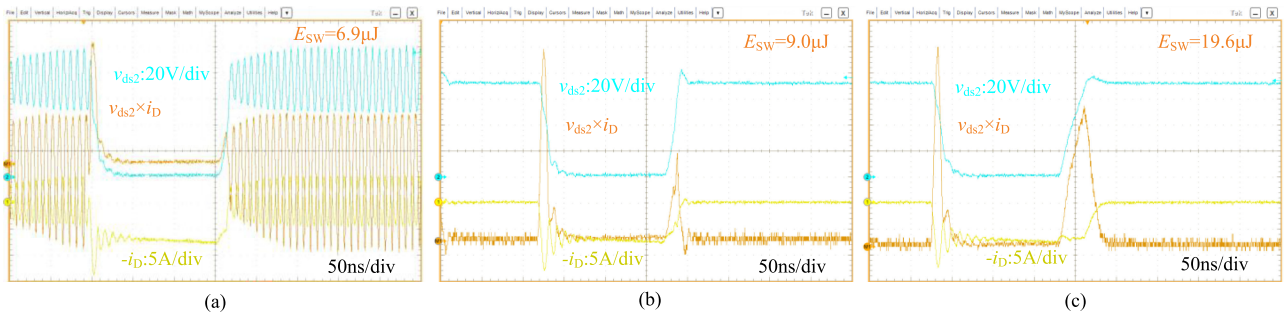

Fig. 21. Energy loss without *RC* and with *RC* snubber circuit ($I_L = 8$ A). (a) Without *RC* snubber. (b) With *RC* snubber (point *S*). (c) With *RC* snubber (point *S*1).

Fig. 16 shows the experimental results without and with the *RC* snubber. When the *RC* snubber is adopted, the sustained oscillation of v_{ds2} can be well suppressed. Fig. 17 shows the experimental verification results within the designed *RC* region and outside the region. It can be observed that the oscillation can be suppressed satisfactorily within the region (point *S* and point *S*1). However, whether R_{snb} is larger (point *B*), smaller (point *A*) or C_{snb} is smaller (point *C*), the experimental results indicate that they have longer oscillation time. The final experimental results are consistent with the theoretical analysis and simulation results. These results support our conclusion that the well oscillation suppression effect can be obtained by an elaborately designed *RC* snubber circuit.

Fig. 18 shows the sustained oscillation suppression effect for the proposed *RC* design method under different inductor currents. The *RC* parameter is selected in the fully suppressed region (point *S*1). It can be seen that when the inductor current changes from 4 to 10 A, the sustained oscillation of v_{ds2} can still be fully suppressed, which indicates that the proposed *RC* design method still has satisfied oscillation suppression effect for different load currents.

When the input voltage is different, the point *S* is still in the *RC* design region. In order to further verify the effectiveness of our design method, the sustained oscillation suppression effect for the proposed *RC* design method under different input voltages is shown in Fig. 19. It can be concluded that point *S* can still suppress the sustained oscillation well and has a little effect on the switching speed, which further validates the theoretical analysis.

C. Discussion of Results

According to Fig. 17, although the point *S*1 enables the oscillation to be fully suppressed, it greatly slows down the switching speed, which increases the switching loss. When there is no *RC* snubber, the rise time t_r of v_{ds2} is 14 ns, as illustrated in Fig. 20(a). When the *RC* snubber (point *S*1) is added, the rise time t_r of v_{ds2} is 31 ns, as illustrated in Fig. 20(c). It can be seen that the switching speed is greatly slowed down, but the sustained oscillation can be fully suppressed, which improves the reliability of the system. When the *RC* value is in the well suppressed region (point *S*), the suppression effect is not as good as that of point *S*1, but it still has a satisfactory oscillation suppression effect than those outside the designed *RC* region. The rise time t_r of v_{ds2} is 16 ns, as shown in Fig. 20(b). Obviously, it has little effect on the switching speed but greatly suppresses the sustained oscillation and improves the reliability of the system. Therefore, point *S* may be a better choice. However, whether the *RC* values are selected in the well suppressed region or the fully suppressed region should be determined based on the actual circuit requirements.

D. Loss Analysis Comparison

The effect of the *RC* snubber on energy loss is explored in this section. Fig. 21 shows the test waveforms and the energy losses under the condition that the inductor current is 8 A. The switching energy losses are tested in the 500 ns time range that includes complete turn-ON and turn-OFF processes. When the *RC* snubber is not included, the switching energy loss is 6.9 μJ, as

TABLE III
COMPARISON OF ENERGY LOSS AT DIFFERENT POINTS

	Outside the design region			With snubbers (S)	With snubbers (S1)	No snubbers	Increased loss between S and no snubbers	
	Point A	Point B	Point C					
Current (A)	Switching energy loss (μJ)	Switching energy loss (μJ)	Switching energy loss (μJ)	Switching energy loss (μJ)	Switching energy loss (μJ)	Switching energy loss (μJ)	Increased loss (μJ)	Percentage (%)
4	6.3	5.8	5.7	6.1	16.0	4.4	1.7	38.6
6	8.0	7.2	7.3	7.7	18.4	6.7	1.0	14.9
8	9.6	8.6	8.5	9.0	19.6	6.9	2.1	30.4
10	11.6	10.8	10.7	11.3	22.5	10.8	0.5	4.6

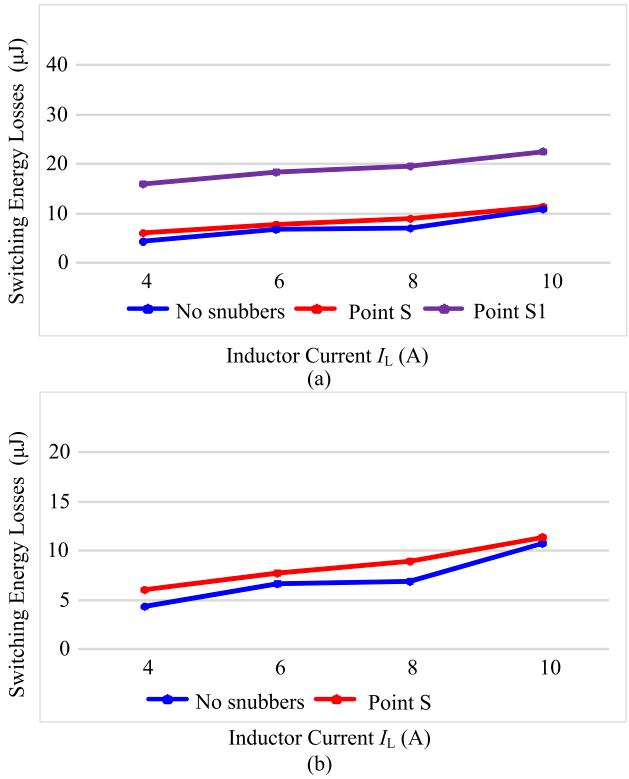

Fig. 22. (a) Comparison of switching energy losses within *RC* design region (point *S* and point *S*1) and without *RC* snubber at different inductor currents. (b) Enlarged view between point *S* and no snubber.

illustrated in Fig. 21(a). When the *RC* snubbers locate at point *S* and point *S*1, the switching energy losses are 9.0 μJ and 19.6 μJ, respectively, as illustrated in Fig. 21(b) and (c). The switching energy losses at different inductor currents within the *RC* design region (point *S* and point *S*1) and without *RC* snubber are given in Table III, and the corresponding comparison of switching energy losses is shown in Fig. 22. It can be seen from Table III that the points *A*, *B,* and *C* outside the design region have similar switching energy losses with the point *S* in the design region. However, their oscillation suppression effect is not as good as point *S*.

It can be concluded that the switching energy losses increase due to the addition of the snubber. In addition, as the inductor current increases, the switching energy losses increase too. According to Fig. 21, the addition of *RC* snubber has a small effect on the turn-ON speed of the device, which mainly slows down the turn-OFF speed of the device and causes an increase in the turn-OFF loss. Although point *S*1 can fully suppress the oscillation, it increases the loss more than that of point *S*. Due to the small cardinality, the relative percentage increase of point *S* in the loss is large when compared with no *RC* snubber. However, it is noteworthy that the absolute increment of point *S* in the loss is very small from Table III and Fig. 22; thus, its effect on the efficiency is negligible. Accordingly, the advantages of the designed *RC* snubber for improving switching characteristics are much more significant than the disadvantages of the increased total loss. Commonly, the smaller the *RC*, the faster the switching speed, and the smaller the switching overlap losses in the transient process, which will reduce the impact on the switching speed and switching energy losses. In addition, the larger the damping ratio, the better the oscillation suppression effect. It can be seen from Fig. 10 and Table III that there is no direct relationship between the damping ratio and the switching energy losses because a large *RC* may also have a small damping ratio but will cause the large switching energy losses. Eventually, reducing the *RC* values in the design region is beneficial to reduce the switching energy losses while also meeting the well oscillation suppression effect.

V. CONCLUSION

In this article, an *RC* method with dipole elimination based on the root locus analysis is adopted to suppress the sustained oscillation for GaN transistors, and the *RC* regions to achieve the well and full suppression effect are quantitatively sketched by using a root locus analysis. It is shown that the oscillation suppression effect within the *RC* design region is better than that outside the *RC* design region. In addition, the sustained oscillation can be fully suppressed with a little increase of switching loss or it can be well suppressed with little influence on switching loss when the *RC* parameters are properly chosen. The simulation and experimental results are consistent with the theoretical analysis, which effectively supports our analytical design. Conclusively, the proposed method indicates a substantial improvement in the switching characteristics and system performance.

The main contributions of this article lie in the following two aspects. On the one hand, it is the first time to adopt the *RC* snubber to suppress this sustained oscillation, which is very simple and cheap but effective; thus, it has a high practical value. On the second hand, dipole elimination is used for the first time to achieve *RC* parameter design in the high-order systems; thus, the oscillation can be suppressed well. This method is instructive for high-order circuits to establish dipoles through circuit design

to achieve oscillation suppression, and the thinking of finding dipoles is also helpful to analyze and improve the performance of high-order systems.

APPENDIX

The coefficients in (16) are shown as follows:

$$a_0 = C_{gd}{}^2C_{oss2}C_{snb}L_2L_GR_{snb}V_0 + C_{gd}{}^2C_{oss2}C_{snb}L_2L_SR_{snb}V_0 + C_{gd}{}^2C_{oss2}C_{snb}I_0L_2L_GR_{loop}R_{snb} + C_{gd}{}^2C_{oss2}C_{snb}I_0L_2L_SR_{loop}R_{snb} - C_{iss}C_{oss}C_{oss2}C_{snb}L_2L_GR_{snb}V_0 - C_{iss}C_{oss}C_{oss2}C_{snb}L_2L_SR_{snb}V_0 - C_{iss}C_{oss}C_{oss2}C_{snb}I_0L_2L_GR_{loop}R_{snb} - C_{iss}C_{oss}C_{oss2}C_{snb}I_0L_2L_SR_{loop}R_{snb}$$

$$a_1 = C_{gd}{}^2C_{oss2}L_2L_GV_0 + C_{gd}{}^2C_{oss2}L_2L_SV_0 - C_{iss}C_{oss}C_{oss2}L_2L_GV_0 - C_{iss}C_{oss}C_{oss2}L_2L_SV_0 + C_{gd}{}^2C_{oss2}I_0L_2L_GR_{loop} + C_{gd}{}^2C_{oss2}I_0L_2L_SR_{loop} - C_{gd}{}^2C_{snb}I_0L_DL_GR_{snb} - C_{gd}{}^2C_{snb}I_0L_DL_SR_{snb} - C_{gd}{}^2C_{snb}I_0L_GL_SR_{snb} - C_{iss}C_{oss}C_{oss2}I_0L_2L_GR_{loop} - C_{iss}C_{oss}C_{oss2}C_{snb}I_0L_2L_GR_{snb} - C_{iss}C_{oss}C_{oss2}I_0L_2L_SR_{loop} + C_{gd}C_{oss2}C_{snb}I_0L_2L_SR_{snb} - C_{iss}C_{oss2}C_{snb}I_0L_2L_SR_{snb} + C_{iss}C_{oss}C_{snb}I_0L_DL_GR_{snb} + C_{iss}C_{oss}C_{snb}I_0L_DL_SR_{snb} + C_{iss}C_{oss}C_{snb}I_0L_GL_SR_{snb} + C_{gd}{}^2C_{oss2}C_{snb}L_2R_GR_{snb}V_0 + C_{gd}{}^2C_{oss2}C_{snb}I_0L_2R_GR_{loop}R_{snb} - C_{iss}C_{oss}C_{oss2}C_{snb}L_2R_GR_{snb}V_0 + C_{gd}C_{oss2}C_{snb}L_2L_GR_{snb}V_0g_m + C_{gd}C_{oss2}C_{snb}I_0L_2L_GR_{loop}R_{snb}g_m - C_{iss}C_{oss2}C_{snb}I_0L_2L_GR_{loop}R_{snb}g_m + C_{gd}C_{oss2}C_{snb}I_0L_2L_SR_{loop}R_{snb}g_m - C_{iss}C_{oss2}C_{snb}I_0L_2L_SR_{loop}R_{snb}g_m - C_{iss}C_{oss}C_{oss2}C_{snb}I_0L_2R_GR_{loop}R_{snb}$$

$$a_2 = C_{gd}{}^2C_{oss2}L_2R_GV_0 - C_{gd}{}^2I_0L_DL_S - C_{gd}{}^2I_0L_GL_S - C_{gd}{}^2I_0L_DL_G + C_{gd}{}^2C_{snb}L_GR_{snb}V_0 + C_{gd}{}^2C_{snb}L_SR_{snb}V_0 - C_{iss}C_{oss2}I_0L_2L_G + C_{gd}C_{oss2}I_0L_2L_S - C_{iss}C_{oss2}I_0L_2L_S + C_{iss}C_{oss}I_0L_DL_G + C_{iss}C_{oss}I_0L_DL_S + C_{iss}C_{oss}I_0L_GL_S - C_{iss}C_{oss}C_{oss2}L_2R_GV_0 - C_{oss}C_{oss2}C_{snb}L_2R_{snb}V_0 - C_{iss}C_{oss}C_{snb}L_GR_{snb}V_0 - C_{iss}C_{oss}C_{snb}L_SR_{snb}V_0 + C_{gd}C_{oss2}L_2L_GV_0g_m + C_{gd}{}^2C_{oss2}I_0L_2R_GR_{loop} - C_{gd}{}^2C_{snb}I_0L_DR_GR_{snb} - C_{gd}{}^2C_{snb}I_0L_SR_GR_{snb} - C_{iss}C_{oss}C_{oss2}I_0L_2R_GR_{loop} - C_{iss}C_{oss2}C_{snb}I_0L_2R_GR_{snb} - C_{oss}C_{oss2}C_{snb}I_0L_2R_{loop}R_{snb} + C_{iss}C_{oss}C_{snb}I_0L_DR_GR_{snb} + C_{iss}C_{oss}C_{snb}I_0L_SR_GR_{snb} + C_{gd}C_{oss2}I_0L_2L_GR_{loop}g_m - C_{iss}C_{oss2}I_0L_2L_GR_{loop}g_m + C_{gd}C_{oss2}I_0L_2L_SR_{loop}g_m - C_{iss}C_{oss2}I_0L_2L_SR_{loop}g_m - C_{gd}C_{snb}I_0L_DL_GR_{snb}g_m + C_{iss}C_{snb}I_0L_DL_GR_{snb}g_m - C_{gd}C_{snb}I_0L_DL_SR_{snb}g_m + C_{iss}C_{snb}I_0L_DL_SR_{snb}g_m - C_{gd}C_{snb}I_0L_GL_SR_{snb}g_m + C_{iss}C_{snb}I_0L_GL_SR_{snb}g_m + C_{gd}C_{oss2}C_{snb}L_2R_GR_{snb}V_0g_m + C_{gd}C_{oss2}C_{snb}I_0L_2R_GR_{loop}R_{snb}g_m - C_{iss}C_{oss2}C_{snb}I_0L_2R_GR_{loop}R_{snb}g_m$$

$$a_3 = C_{gd}{}^2L_GV_0 + C_{gd}{}^2L_SV_0 - C_{oss}C_{oss2}L_2V_0 - C_{iss}C_{oss}L_GV_0 - C_{iss}C_{oss}L_SV_0 - C_{gd}{}^2I_0L_DR_G - C_{gd}{}^2I_0L_SR_G + C_{gd}{}^2C_{snb}R_GR_{snb}V_0 - C_{iss}C_{oss2}I_0L_2R_G - C_{oss}C_{oss2}I_0L_2R_{loop} - C_{oss2}C_{snb}I_0L_2R_{snb} + C_{iss}C_{oss}I_0L_DR_G + C_{iss}C_{oss}I_0L_SR_G + C_{oss}C_{snb}I_0L_DR_{snb} - C_{gd}C_{snb}I_0L_SR_{snb} + C_{oss}C_{snb}I_0L_SR_{snb} - C_{gd}I_0L_DL_Gg_m + C_{iss}I_0L_DL_Gg_m - C_{gd}I_0L_DL_Sg_m + C_{iss}I_0L_DL_Sg_m - C_{gd}I_0L_GL_Sg_m + C_{iss}I_0L_GL_Sg_m - C_{iss}C_{oss}C_{snb}R_GR_{snb}V_0 + C_{gd}C_{oss2}L_2R_GV_0g_m + C_{gd}C_{snb}L_GR_{snb}V_0g_m + C_{gd}C_{oss2}I_0L_2R_GR_{loop}g_m - C_{iss}C_{oss2}I_0L_2R_GR_{loop}g_m - C_{oss2}C_{snb}I_0L_2R_{loop}R_{snb}g_m - C_{gd}C_{snb}I_0L_DR_GR_{snb}g_m + C_{iss}C_{snb}I_0L_DR_GR_{snb}g_m - C_{gd}C_{snb}I_0L_SR_GR_{snb}g_m + C_{iss}C_{snb}I_0L_SR_GR_{snb}g_m$$

$$a_4 = C_{oss}I_0L_D - C_{oss2}I_0L_2 - C_{gd}I_0L_S + C_{oss}I_0L_S + C_{gd}{}^2R_GV_0 - C_{iss}C_{oss}R_GV_0 - C_{oss}C_{snb}R_{snb}V_0 + C_{gd}L_GV_0g_m - C_{oss2}I_0L_2R_{loop}g_m - C_{gd}I_0L_DR_Gg_m + C_{iss}I_0L_DR_Gg_m - C_{gd}I_0L_SR_Gg_m + C_{iss}I_0L_SR_Gg_m + C_{snb}I_0L_DR_{snb}g_m + C_{gd}C_{snb}R_GR_{snb}V_0g_m$$

$$a_5 = -C_{oss}V_0 + I_0L_Dg_m + C_{gd}R_GV_0g_m$$

$$b_0 = C_{iss}C_{oss}C_{oss2}C_{snb}L_2L_DL_G - C_{gd}{}^2C_{oss2}C_{snb}L_2L_DL_S - C_{gd}{}^2C_{oss2}C_{snb}L_2L_GL_S - C_{gd}{}^2C_{oss2}C_{snb}L_2L_DL_G + C_{iss}C_{oss}C_{oss2}C_{snb}L_2L_DL_S + C_{iss}C_{oss}C_{oss2}C_{snb}L_2L_GL_S$$

$$b_1 = C_{iss}C_{oss}C_{oss2}C_{snb}L_2L_DR_G - C_{gd}{}^2C_{oss2}C_{snb}L_2L_GR_{loop} - C_{gd}{}^2C_{oss2}C_{snb}L_2L_SR_G - C_{gd}{}^2C_{oss2}C_{snb}L_2L_GR_{snb} - C_{gd}{}^2C_{oss2}C_{snb}L_2L_SR_{loop} - C_{gd}{}^2C_{oss2}C_{snb}L_2L_SR_{snb} - C_{gd}{}^2C_{oss2}C_{snb}L_DL_GR_{snb} - C_{gd}{}^2C_{oss2}C_{snb}L_DL_SR_{snb} - C_{gd}{}^2C_{oss2}C_{snb}L_GL_SR_{snb} - C_{gd}{}^2C_{oss2}C_{snb}L_2L_DR_G + C_{iss}C_{oss}C_{oss2}C_{snb}L_2L_GR_{loop} + C_{iss}C_{oss}C_{oss2}C_{snb}L_2L_SR_G + C_{iss}C_{oss}C_{oss2}C_{snb}L_2L_GR_{snb} + C_{iss}C_{oss}C_{oss2}C_{snb}L_2L_SR_{loop} + C_{iss}C_{oss}C_{oss2}C_{snb}L_2L_SR_{snb} + C_{iss}C_{oss}C_{oss2}C_{snb}L_DL_GR_{snb} + C_{iss}C_{oss}C_{oss2}C_{snb}L_DL_SR_{snb} + C_{iss}C_{oss}C_{oss2}C_{snb}L_GL_SR_{snb} - C_{gd}C_{oss2}C_{snb}L_2L_DL_Gg_m + C_{iss}C_{oss2}C_{snb}L_2L_DL_Gg_m - C_{gd}C_{oss2}C_{snb}L_2L_DL_Sg_m + C_{iss}C_{oss2}C_{snb}L_2L_DL_Sg_m - C_{gd}C_{oss2}C_{snb}L_2L_GL_Sg_m + C_{iss}C_{oss2}C_{snb}L_2L_GL_Sg_m$$

$$b_2 = C_{iss}C_{oss}C_{oss2}L_2L_G - C_{gd}{}^2C_{oss2}L_2L_S - C_{gd}{}^2C_{oss2}L_DL_G - C_{gd}{}^2C_{snb}L_DL_G - C_{gd}{}^2C_{oss2}L_DL_S - C_{gd}{}^2C_{oss2}L_GL_S - C_{gd}{}^2C_{snb}L_DL_S - C_{gd}{}^2C_{snb}L_GL_S - C_{gd}{}^2C_{oss2}L_2L_G + C_{iss}C_{oss2}C_{snb}L_2L_G + C_{oss}C_{oss2}C_{snb}L_2L_D + C_{iss}C_{oss}C_{oss2}L_2L_S - 2C_{gd}C_{oss2}C_{snb}L_2L_S + C_{iss}C_{oss2}C_{snb}L_2L_S + C_{oss}C_{oss2}C_{snb}L_2L_S + C_{iss}C_{oss}C_{oss2}L_DL_G + C_{iss}C_{oss}C_{snb}L_DL_G + C_{iss}C_{oss}C_{oss2}L_DL_S + C_{iss}C_{oss}C_{oss2}L_GL_S + C_{iss}C_{oss}C_{snb}L_DL_S + C_{iss}C_{oss}C_{snb}L_GL_S - C_{gd}{}^2C_{oss2}C_{snb}L_2R_GR_{loop} - C_{gd}{}^2C_{oss2}C_{snb}L_2R_GR_{snb} - C_{gd}{}^2C_{oss2}C_{snb}L_DR_GR_{snb} - C_{gd}{}^2C_{oss2}C_{snb}L_GR_{loop}R_{snb} - C_{gd}{}^2C_{oss2}C_{snb}L_SR_GR_{snb} - C_{gd}{}^2C_{oss2}C_{snb}L_SR_{loop}R_{snb} + C_{iss}C_{oss}C_{oss2}C_{snb}L_2R_GR_{loop} + C_{iss}C_{oss}C_{oss2}C_{snb}L_2R_GR_{snb} + C_{iss}C_{oss}C_{oss2}C_{snb}L_DR_GR_{snb} + C_{iss}C_{oss}C_{snb}L_GR_{loop}R_{snb} + C_{iss}C_{oss}C_{oss2}C_{snb}L_SR_GR_{snb} + C_{iss}C_{oss}C_{snb}L_SR_{loop}R_{snb} - C_{gd}C_{oss2}C_{snb}L_2L_DR_Gg_m + C_{iss}C_{oss2}C_{snb}L_2L_DR_Gg_m - C_{gd}C_{oss2}C_{snb}L_2L_GR_{loop}g_m + C_{iss}C_{oss2}C_{snb}L_2L_GR_{loop}g_m - C_{gd}C_{oss2}C_{snb}L_2L_SR_Gg_m - C_{gd}C_{oss2}C_{snb}L_2L_GR_{snb}g_m + C_{iss}C_{oss2}C_{snb}L_2L_SR_Gg_m + C_{iss}C_{oss2}C_{snb}L_2L_GR_{snb}g_m - C_{gd}C_{oss2}C_{snb}L_2L_SR_{loop}g_m + C_{iss}C_{oss2}C_{snb}L_2L_SR_{loop}g_m - C_{gd}C_{oss2}C_{snb}L_2L_SR_{snb}g_m + C_{iss}C_{oss2}C_{snb}L_2L_SR_{snb}g_m - C_{gd}C_{oss2}C_{snb}L_DL_GR_{snb}g_m + C_{iss}C_{oss2}C_{snb}L_DL_GR_{snb}g_m - C_{gd}C_{oss2}C_{snb}L_DL_SR_{snb}g_m + C_{iss}C_{oss2}C_{snb}L_DL_SR_{snb}g_m - C_{gd}C_{oss2}C_{snb}L_GL_SR_{snb}g_m + C_{iss}C_{oss2}C_{snb}L_GL_SR_{snb}g_m$$

$$b_3 = C_{iss}C_{oss}C_{oss2}L_2R_G - C_{gd}{}^2C_{oss2}L_DR_G - C_{gd}{}^2C_{snb}L_DR_G - C_{gd}{}^2C_{oss2}L_GR_{loop} - C_{gd}{}^2C_{snb}L_GR_{loop} - C_{gd}{}^2C_{oss2}L_SR_G - C_{gd}{}^2C_{snb}L_SR_G - C_{gd}{}^2C_{snb}L_GR_{snb} - C_{gd}{}^2C_{oss2}L_SR_{loop} - C_{gd}{}^2C_{snb}L_SR_{loop} - C_{gd}{}^2C_{snb}L_SR_{snb} - C_{gd}{}^2C_{oss2}L_2R_G + C_{iss}C_{oss2}C_{snb}L_2R_G + C_{oss}C_{oss2}C_{snb}L_2R_{loop} + C_{oss}C_{oss2}C_{snb}L_2R_{snb} + C_{iss}C_{oss}C_{oss2}L_DR_G + C_{iss}C_{oss}C_{snb}L_DR_G + C_{iss}C_{oss}C_{oss2}L_GR_{loop} + C_{iss}C_{oss}C_{snb}L_GR_{loop} + C_{iss}C_{oss}C_{oss2}L_SR_G + C_{iss}C_{oss}C_{snb}L_SR_G + C_{iss}C_{oss}C_{snb}L_GR_{snb} + C_{iss}C_{oss2}C_{snb}L_GR_{snb} +$$

$C_{oss}C_{oss2}C_{snb}L_DR_{snb} + C_{iss}C_{oss}C_{oss2}L_SR_{loop} + C_{iss}C_{oss}C_{snb}L_SR_{loop} - 2C_{gd}C_{oss2}C_{snb}L_SR_{snb} + C_{iss}C_{oss}C_{snb}L_SR_{snb} + C_{iss}C_{oss2}C_{snb}L_SR_{snb} + C_{oss}C_{oss2}C_{snb}L_SR_{snb} - C_{gd}C_{oss2}L_2L_GL_Gg_m + C_{iss}C_{oss2}L_2L_Gg_m + C_{oss2}C_{snb}L_2L_Dg_m - C_{gd}C_{oss2}L_2L_Sg_m + C_{iss}C_{oss2}L_2L_Sg_m - C_{gd}C_{oss2}L_DL_Gg_m + C_{iss}C_{oss2}L_DL_Gg_m - C_{gd}C_{snb}L_DL_Gg_m + C_{iss}C_{snb}L_DL_Gg_m - C_{gd}C_{oss2}L_DL_Sg_m + C_{iss}C_{oss2}L_DL_Sg_m - C_{gd}C_{oss2}L_GL_Sg_m - C_{gd}C_{snb}L_DL_Sg_m + C_{iss}C_{oss2}L_GL_Sg_m + C_{iss}C_{snb}L_DL_Sg_m - C_{gd}C_{snb}L_GL_Sg_m + C_{iss}C_{snb}L_GL_Sg_m - C_{gd}{}^2C_{oss2}C_{snb}R_GR_{loop}R_{snb} + C_{iss}C_{oss}C_{oss2}C_{snb}R_GR_{loop}R_{snb} - C_{gd}C_{oss2}C_{snb}L_2R_GR_{loop}g_m + C_{iss}C_{oss2}C_{snb}L_2R_GR_{loop}g_m - C_{gd}C_{oss2}C_{snb}L_2R_GR_{snb}g_m + C_{iss}C_{oss2}C_{snb}L_2R_GR_{snb}g_m - C_{gd}C_{oss2}C_{snb}L_DR_GR_{snb}g_m + C_{iss}C_{oss2}C_{snb}L_DR_GR_{snb}g_m - C_{gd}C_{oss2}C_{snb}L_GR_{loop}R_{snb}g_m + C_{iss}C_{oss2}C_{snb}L_GR_{loop}R_{snb}g_m - C_{gd}C_{oss2}C_{snb}L_SR_GR_{snb}g_m + C_{iss}C_{oss2}C_{snb}L_SR_GR_{snb}g_m - C_{gd}C_{oss2}C_{snb}L_SR_{loop}R_{snb}g_m + C_{iss}C_{oss2}C_{snb}L_SR_{loop}R_{snb}g_m$

$b_4 = C_{oss}C_{oss2}L_2 - C_{gd}{}^2L_S - C_{gd}{}^2L_G + C_{oss2}C_{snb}L_2 + C_{iss}C_{oss}L_G + C_{iss}C_{oss2}L_G + C_{oss}C_{oss2}L_D + C_{iss}C_{snb}L_G + C_{oss}C_{snb}L_D - 2C_{gd}C_{oss2}L_S + C_{iss}C_{oss}L_S + C_{iss}C_{oss2}L_S - 2C_{gd}C_{snb}L_S + C_{iss}C_{snb}L_S + C_{oss}C_{oss2}L_S + C_{oss}C_{snb}L_S - C_{gd}{}^2C_{oss2}R_GR_{loop} - C_{gd}{}^2C_{snb}R_GR_{loop} - C_{gd}{}^2C_{snb}R_GR_{snb} + C_{iss}C_{oss}C_{oss2}R_GR_{loop} + C_{iss}C_{oss}C_{snb}R_GR_{loop} + C_{iss}C_{oss}C_{snb}R_GR_{snb} + C_{iss}C_{oss2}C_{snb}R_GR_{snb} + C_{oss}C_{oss2}C_{snb}R_{loop}R_{snb} - C_{gd}C_{oss2}L_2R_Gg_m + C_{iss}C_{oss2}L_2R_Gg_m + C_{oss2}C_{snb}L_2R_{loop}g_m + C_{oss2}C_{snb}L_2R_{snb}g_m - C_{gd}C_{oss2}L_DR_Gg_m + C_{iss}C_{oss2}L_DR_Gg_m - C_{gd}C_{snb}L_DR_Gg_m + C_{iss}C_{snb}L_DR_Gg_m - C_{gd}C_{oss2}L_GR_{loop}g_m + C_{iss}C_{oss2}L_GR_{loop}g_m - C_{gd}C_{snb}L_GR_{loop}g_m + C_{iss}C_{snb}L_GR_{loop}g_m - C_{gd}C_{oss2}L_SR_Gg_m + C_{iss}C_{oss2}L_SR_Gg_m - C_{gd}C_{snb}L_SR_Gg_m - C_{gd}C_{snb}L_GR_{snb}g_m + C_{iss}C_{snb}L_SR_Gg_m + C_{iss}C_{snb}L_GR_{snb}g_m + C_{oss2}C_{snb}L_DR_{snb}g_m - C_{gd}C_{oss2}L_SR_{loop}g_m + C_{iss}C_{oss2}L_SR_{loop}g_m - C_{gd}C_{snb}L_SR_{loop}g_m + C_{iss}C_{snb}L_SR_{loop}g_m - C_{gd}C_{snb}L_SR_{snb}g_m + C_{iss}C_{snb}L_SR_{snb}g_m - C_{gd}C_{oss2}C_{snb}R_GR_{loop}R_{snb}g_m + C_{iss}C_{oss2}C_{snb}R_GR_{loop}R_{snb}g_m$

$b_5 = C_{iss}C_{oss}R_G - C_{gd}{}^2R_G + C_{iss}C_{oss2}R_G + C_{iss}C_{snb}R_G + C_{oss}C_{oss2}R_{loop} + C_{oss}C_{snb}R_{loop} + C_{oss}C_{snb}R_{snb} + C_{oss2}C_{snb}R_{snb} + C_{oss2}L_2g_m - C_{gd}L_Gg_m + C_{iss}L_Gg_m + C_{oss2}L_Dg_m + C_{snb}L_Dg_m - C_{gd}L_Sg_m + C_{iss}L_Sg_m - C_{gd}C_{oss2}R_GR_{loop}g_m + C_{iss}C_{oss2}R_GR_{loop}g_m - C_{gd}C_{snb}R_GR_{loop}g_m + C_{iss}C_{snb}R_GR_{loop}g_m - C_{gd}C_{snb}R_GR_{snb}g_m + C_{iss}C_{snb}R_GR_{snb}g_m + C_{oss2}C_{snb}R_{loop}R_{snb}g_m$

$b_6 = C_{oss} + C_{oss2} + C_{snb} - C_{gd}R_Gg_m + C_{iss}R_Gg_m + C_{oss2}R_{loop}g_m + C_{snb}R_{loop}g_m + C_{snb}R_{snb}g_m$

$b_7 = g_m$.

The coefficients in (20) are shown as follows:

$Q = (C_{iss}C_{oss}C_{oss2}L_2L_DL_G - C_{gd}{}^2C_{oss2}L_2L_DL_S - C_{gd}{}^2C_{oss2}L_2L_GL_S - C_{gd}{}^2C_{oss2}L_2L_DL_G + C_{iss}C_{oss}C_{oss2}L_2L_DL_S + C_{iss}C_{oss}C_{oss2}L_2L_GL_S)s^7 + (C_{iss}C_{oss}C_{oss2}L_2L_DR_G - C_{gd}{}^2C_{oss2}L_2L_GR_{loop} - C_{gd}{}^2C_{oss2}L_2L_SR_G - C_{gd}{}^2C_{oss2}L_2L_GR_{snb} - C_{gd}{}^2C_{oss2}L_2L_SR_{loop} - C_{gd}{}^2C_{oss2}L_2L_SR_{snb} - C_{gd}{}^2C_{oss2}L_DL_GR_{snb} - C_{gd}{}^2C_{oss2}L_DL_SR_{snb} - C_{gd}{}^2C_{oss2}L_GL_SR_{snb} - C_{gd}{}^2C_{oss2}L_2L_DR_G + C_{iss}C_{oss}C_{oss2}L_2L_GR_{loop} + C_{iss}C_{oss}C_{oss2}L_2L_SR_G + C_{iss}C_{oss}C_{oss2}L_2L_GR_{snb} + C_{iss}C_{oss}C_{oss2}L_2L_SR_{loop} + C_{iss}C_{oss}C_{oss2}L_2L_SR_{snb} + C_{iss}C_{oss}C_{oss2}L_DL_GR_{snb} + C_{iss}C_{oss}C_{oss2}L_DL_SR_{snb} + C_{iss}C_{oss}C_{oss2}L_GL_SR_{snb} - C_{gd}C_{oss2}L_2L_DL_Gg_m + C_{iss}C_{oss2}L_2L_DL_Gg_m - C_{gd}C_{oss2}L_2L_DL_Sg_m + C_{iss}C_{oss2}L_2L_DL_Sg_m - C_{gd}C_{oss2}L_2L_GL_Sg_m + C_{iss}C_{oss2}L_2L_GL_Sg_m)s^6 + (C_{iss}C_{oss2}L_2L_G - C_{gd}{}^2L_DL_S - C_{gd}{}^2L_GL_S - C_{gd}{}^2L_DL_G + C_{oss}C_{oss2}L_2L_D - 2C_{gd}C_{oss2}L_2L_S + C_{iss}C_{oss2}L_2L_S + C_{oss}C_{oss2}L_2L_S + C_{iss}C_{oss}L_DL_G + C_{iss}C_{oss}L_DL_S + C_{iss}C_{oss}L_GL_S - C_{gd}{}^2C_{oss2}L_2R_GR_{loop} - C_{gd}{}^2C_{oss2}L_2R_GR_{snb} - C_{gd}{}^2C_{oss2}L_DR_GR_{snb} - C_{gd}{}^2C_{oss2}L_GR_{loop}R_{snb} - C_{gd}{}^2C_{oss2}L_SR_GR_{snb} - C_{gd}{}^2C_{oss2}L_SR_{loop}R_{snb} + C_{iss}C_{oss}C_{oss2}L_2R_GR_{loop} + C_{iss}C_{oss}C_{oss2}L_2R_GR_{snb} + C_{iss}C_{oss}C_{oss2}L_DR_GR_{snb} + C_{iss}C_{oss}C_{oss2}L_GR_{loop}R_{snb} + C_{iss}C_{oss}C_{oss2}L_SR_GR_{snb} + C_{iss}C_{oss}C_{oss2}L_SR_{loop}R_{snb} - C_{gd}C_{oss2}L_2L_DR_Gg_m + C_{iss}C_{oss2}L_2L_DR_Gg_m - C_{gd}C_{oss2}L_2L_GR_{loop}g_m + C_{iss}C_{oss2}L_2L_GR_{loop}g_m - C_{gd}C_{oss2}L_2L_SR_Gg_m - C_{gd}C_{oss2}L_2L_GR_{snb}g_m + C_{iss}C_{oss2}L_2L_SR_Gg_m + C_{iss}C_{oss2}L_2L_GR_{snb}g_m - C_{gd}C_{oss2}L_2L_SR_{loop}g_m + C_{iss}C_{oss2}L_2L_SR_{loop}g_m - C_{gd}C_{oss2}L_2L_SR_{snb}g_m + C_{iss}C_{oss2}L_2L_SR_{snb}g_m - C_{gd}C_{oss2}L_DL_GR_{snb}g_m + C_{iss}C_{oss2}L_DL_GR_{snb}g_m - C_{gd}C_{oss2}L_DL_SR_{snb}g_m + C_{iss}C_{oss2}L_DL_SR_{snb}g_m - C_{gd}C_{oss2}L_GL_SR_{snb}g_m + C_{iss}C_{oss2}L_GL_SR_{snb}g_m)s^5 + (C_{iss}C_{oss2}L_2R_G - C_{gd}{}^2L_GR_{loop} - C_{gd}{}^2L_SR_G - C_{gd}{}^2L_GR_{snb} - C_{gd}{}^2L_SR_{loop} - C_{gd}{}^2L_SR_{snb} - C_{gd}{}^2L_DR_G + C_{oss}C_{oss2}L_2R_{loop} + C_{oss}C_{oss2}L_2R_{snb} + C_{iss}C_{oss}L_DR_G + C_{iss}C_{oss}L_GR_{loop} + C_{iss}C_{oss}L_SR_G + C_{iss}C_{oss}L_GR_{snb} + C_{iss}C_{oss2}L_GR_{snb} + C_{oss}C_{oss2}L_DR_{snb} + C_{iss}C_{oss}L_SR_{loop} - 2C_{gd}C_{oss2}L_SR_{snb} + C_{iss}C_{oss}L_SR_{snb} + C_{iss}C_{oss2}L_SR_{snb} + C_{oss}C_{oss2}L_SR_{snb} + C_{oss2}L_2L_Dg_m - C_{gd}L_DL_Gg_m + C_{iss}L_DL_Gg_m - C_{gd}L_DL_Sg_m + C_{iss}L_DL_Sg_m - C_{gd}L_GL_Sg_m + C_{iss}L_GL_Sg_m - C_{gd}{}^2C_{oss2}R_GR_{loop}R_{snb} + C_{iss}C_{oss}C_{oss2}R_GR_{loop}R_{snb} - C_{gd}C_{oss2}L_2R_GR_{loop}g_m + C_{iss}C_{oss2}L_2R_GR_{loop}g_m - C_{gd}C_{oss2}L_2R_GR_{snb}g_m + C_{iss}C_{oss2}L_2R_GR_{snb}g_m - C_{gd}C_{oss2}L_DR_GR_{snb}g_m + C_{iss}C_{oss2}L_DR_GR_{snb}g_m - C_{gd}C_{oss2}L_GR_{loop}R_{snb}g_m + C_{iss}C_{oss2}L_GR_{loop}R_{snb}g_m - C_{gd}C_{oss2}L_SR_GR_{snb}g_m + C_{iss}C_{oss2}L_SR_GR_{snb}g_m - C_{gd}C_{oss2}L_SR_{loop}R_{snb}g_m + C_{iss}C_{oss2}L_SR_{loop}R_{snb}g_m)s^4 + (C_{oss2}L_2 + C_{iss}L_G + C_{oss}L_D - 2C_{gd}L_S + C_{iss}L_S + C_{oss}L_S - C_{gd}{}^2R_GR_{loop} - C_{gd}{}^2R_GR_{snb} + C_{iss}C_{oss}R_GR_{loop} + C_{iss}C_{oss}R_GR_{snb} + C_{iss}C_{oss2}R_GR_{snb} + C_{oss}C_{oss2}R_{loop}R_{snb} + C_{oss2}L_2R_{loop}g_m + C_{oss2}L_2R_{snb}g_m - C_{gd}L_DR_Gg_m + C_{iss}L_DR_Gg_m - C_{gd}L_GR_{loop}g_m + C_{iss}L_GR_{loop}g_m - C_{gd}L_SR_Gg_m - C_{gd}L_GR_{snb}g_m + C_{iss}L_SR_Gg_m + C_{iss}L_GR_{snb}g_m + C_{oss2}L_DR_{snb}g_m - C_{gd}L_SR_{loop}g_m + C_{iss}L_SR_{loop}g_m - C_{gd}L_SR_{snb}g_m + C_{iss}L_SR_{snb}g_m - C_{gd}C_{oss2}R_GR_{loop}R_{snb}g_m + C_{iss}C_{oss2}R_GR_{loop}R_{snb}g_m)s^3 + (L_Dg_m + C_{iss}R_G + C_{oss}R_{loop} + C_{oss}R_{snb} + C_{oss2}R_{snb} - C_{gd}R_GR_{loop}g_m + C_{iss}R_GR_{loop}g_m - C_{gd}R_GR_{snb}g_m + C_{iss}R_GR_{snb}g_m + C_{oss2}R_{loop}R_{snb}g_m)s^2 + (R_{loop}g_m + R_{snb}g_m + 1)s$

$P = (C_{iss}C_{oss}C_{oss2}L_2L_G - C_{gd}{}^2C_{oss2}L_2L_S - C_{gd}{}^2C_{oss2}L_DL_G - C_{gd}{}^2C_{oss2}L_DL_S - C_{gd}{}^2C_{oss2}L_GL_S - C_{gd}{}^2C_{oss2}L_2L_G + C_{iss}C_{oss}C_{oss2}L_2L_S + C_{iss}C_{oss}C_{oss2}L_DL_G + C_{iss}C_{oss}C_{oss2}L_DL_S + C_{iss}C_{oss}C_{oss2}L_GL_S)s^5 + (C_{iss}C_{oss}C_{oss2}L_2R_G - C_{gd}{}^2C_{oss2}L_DR_G - C_{gd}{}^2C_{oss2}L_GR_{loop} - C_{gd}{}^2C_{oss2}L_SR_G - C_{gd}{}^2C_{oss2}L_SR_{loop} - C_{gd}{}^2C_{oss2}L_2R_G$

$+ C_{iss}C_{oss}C_{oss2}L_DR_G + C_{iss}C_{oss}C_{oss2}L_GR_{loop} + C_{iss}C_{oss}C_{oss2}L_SR_G + C_{iss}C_{oss}C_{oss2}L_SR_{loop} - C_{gd}C_{oss2}L_2L_Gg_m + C_{iss}C_{oss2}L_2L_Gg_m - C_{gd}C_{oss2}L_2L_Sg_m + C_{iss}C_{oss2}L_2L_Sg_m - C_{gd}C_{oss2}L_DL_Gg_m + C_{iss}C_{oss2}L_DL_Gg_m - C_{gd}C_{oss2}L_DL_Sg_m + C_{iss}C_{oss2}L_DL_Sg_m - C_{gd}C_{oss2}L_GL_Sg_m + C_{iss}C_{oss2}L_GL_Sg_m)s^4 + (C_{oss}C_{oss2}L_2 - C_{gd}{}^2L_S - C_{gd}{}^2L_G + C_{iss}C_{oss}L_G + C_{iss}C_{oss2}L_G + C_{oss}C_{oss2}L_D - 2C_{gd}C_{oss2}L_S + C_{iss}C_{oss}L_S + C_{iss}C_{oss2}L_S + C_{oss}C_{oss2}L_S - C_{gd}{}^2C_{oss2}R_GR_{loop} + C_{iss}C_{oss}C_{oss2}R_GR_{loop} - C_{gd}C_{oss2}L_2R_Gg_m + C_{iss}C_{oss2}L_2R_Gg_m - C_{gd}C_{oss2}L_DR_Gg_m + C_{iss}C_{oss2}L_DR_Gg_m - C_{gd}C_{oss2}L_GR_{loop}g_m + C_{iss}C_{oss2}L_GR_{loop}g_m - C_{gd}C_{oss2}L_SR_Gg_m + C_{iss}C_{oss2}L_SR_Gg_m - C_{gd}C_{oss2}L_SR_{loop}g_m + C_{iss}C_{oss2}L_SR_{loop}g_m)s^3 + (C_{iss}C_{oss}R_G - C_{gd}{}^2R_G + C_{iss}C_{oss2}R_G + C_{oss}C_{oss2}R_{loop} + C_{oss2}L_2g_m - C_{gd}L_Gg_m + C_{iss}L_Gg_m + C_{oss2}L_Dg_m - C_{gd}L_Sg_m + C_{iss}L_Sg_m - C_{gd}C_{oss2}R_GR_{loop}g_m + C_{iss}C_{oss2}R_GR_{loop}g_m)s^2 + (C_{oss} + C_{oss2} - C_{gd}R_Gg_m + C_{iss}R_Gg_m + C_{oss2}R_{loop}g_m)s + g_m.$

The coefficients in (21) are shown as follows:

$Q_1 = (C_{gd}{}^2C_{oss2}L_2L_GR_{snb}V_0 + C_{gd}{}^2C_{oss2}L_2L_SR_{snb}V_0 - C_{iss}C_{oss}C_{oss2}L_2L_GR_{snb}V_0 - C_{iss}C_{oss}C_{oss2}L_2L_SR_{snb}V_0 + C_{gd}{}^2C_{oss2}I_0L_2L_GR_{loop}R_{snb} + C_{gd}{}^2C_{oss2}I_0L_2L_SR_{loop}R_{snb} - C_{iss}C_{oss}C_{oss2}I_0L_2L_GR_{loop}R_{snb} - C_{iss}C_{oss}C_{oss2}I_0L_2L_SR_{loop}R_{snb})s^5 + (C_{gd}C_{oss2}I_0L_2L_SR_{snb} - C_{gd}{}^2I_0L_DL_SR_{snb} - C_{gd}{}^2I_0L_GL_SR_{snb} - C_{iss}C_{oss2}I_0L_2L_GR_{snb} - C_{gd}{}^2I_0L_DL_GR_{snb} - C_{iss}C_{oss2}I_0L_2L_SR_{snb} + C_{iss}C_{oss}I_0L_DL_GR_{snb} + C_{iss}C_{oss}I_0L_DL_SR_{snb} + C_{iss}C_{oss}I_0L_GL_SR_{snb} + C_{gd}{}^2C_{oss2}L_2R_GR_{snb}V_0 - C_{iss}C_{oss}C_{oss2}L_2R_GR_{snb}V_0 + C_{gd}C_{oss2}L_2L_GR_{snb}V_0g_m + C_{gd}{}^2C_{oss2}I_0L_2R_GR_{loop}R_{snb} - C_{iss}C_{oss}C_{oss2}I_0L_2R_GR_{loop}R_{snb} + C_{gd}C_{oss2}I_0L_2L_GR_{loop}R_{snb}g_m - C_{iss}C_{oss2}I_0L_2L_GR_{loop}R_{snb}g_m + C_{gd}C_{oss2}I_0L_2L_SR_{loop}R_{snb}g_m - C_{iss}C_{oss2}I_0L_2L_SR_{loop}R_{snb}g_m)s^4 + (C_{gd}{}^2L_GR_{snb}V_0 + C_{gd}{}^2L_SR_{snb}V_0 - C_{gd}{}^2I_0L_DR_GR_{snb} - C_{gd}{}^2I_0L_SR_GR_{snb} - C_{oss}C_{oss2}L_2R_{snb}V_0 - C_{iss}C_{oss}L_GR_{snb}V_0 - C_{iss}C_{oss}L_SR_{snb}V_0 - C_{iss}C_{oss2}I_0L_2R_GR_{snb} - C_{oss}C_{oss2}I_0L_2R_{loop}R_{snb} + C_{iss}C_{oss}I_0L_DR_GR_{snb} + C_{iss}C_{oss}I_0L_SR_GR_{snb} - C_{gd}I_0L_DL_GR_{snb}g_m + C_{iss}I_0L_DL_GR_{snb}g_m - C_{gd}I_0L_DL_SR_{snb}g_m + C_{iss}I_0L_DL_SR_{snb}g_m - C_{gd}I_0L_GL_SR_{snb}g_m + C_{iss}I_0L_GL_SR_{snb}g_m + C_{gd}C_{oss2}L_2R_GR_{snb}V_0g_m + C_{gd}C_{oss2}I_0L_2R_GR_{loop}R_{snb}g_m - C_{iss}C_{oss2}I_0L_2R_GR_{loop}R_{snb}g_m)s^3 + (I_0L_DR_{snb}g_m - C_{oss}R_{snb}V_0 + C_{gd}R_GR_{snb}V_0g_m)s$

$P_1 = (C_{gd}{}^2C_{oss2}L_2L_GV_0 + C_{gd}{}^2C_{oss2}L_2L_SV_0 - C_{iss}C_{oss}C_{oss2}L_2L_GV_0 - C_{iss}C_{oss}C_{oss2}L_2L_SV_0 + C_{gd}{}^2C_{oss2}I_0L_2L_GR_{loop} + C_{gd}{}^2C_{oss2}I_0L_2L_SR_{loop} - C_{iss}C_{oss}C_{oss2}I_0L_2L_GR_{loop} - C_{iss}C_{oss}C_{oss2}I_0L_2L_SR_{loop})s^4 + (C_{gd}{}^2C_{oss2}L_2R_GV_0 - C_{gd}{}^2I_0L_DL_S - C_{gd}{}^2I_0L_GL_S - C_{gd}{}^2I_0L_DL_G - C_{iss}C_{oss2}I_0L_2L_G + C_{gd}C_{oss2}I_0L_2L_S - C_{iss}C_{oss2}I_0L_2L_S + C_{iss}C_{oss}I_0L_DL_G + C_{iss}C_{oss}I_0L_DL_S + C_{iss}C_{oss}I_0L_GL_S - C_{iss}C_{oss}C_{oss2}L_2R_GV_0 + C_{gd}C_{oss2}L_2L_GV_0g_m + C_{gd}{}^2C_{oss2}I_0L_2R_GR_{loop} - C_{iss}C_{oss}C_{oss2}I_0L_2R_GR_{loop} + C_{gd}C_{oss2}I_0L_2L_GR_{loop}g_m - C_{iss}C_{oss2}I_0L_2L_GR_{loop}g_m + C_{gd}C_{oss2}I_0L_2L_SR_{loop}g_m - C_{iss}C_{oss2}I_0L_2L_SR_{loop}g_m)s^3 + (C_{gd}{}^2L_GV_0 + C_{gd}{}^2L_SV_0 - C_{oss}C_{oss2}L_2V_0 - C_{iss}C_{oss}L_GV_0 - C_{iss}C_{oss}L_SV_0 - C_{gd}{}^2I_0L_DR_G - C_{gd}{}^2I_0L_SR_G - C_{iss}C_{oss2}I_0L_2R_G - C_{oss}C_{oss2}I_0L_2R_{loop} + C_{iss}C_{oss}I_0L_DR_G + C_{iss}C_{oss}I_0L_SR_G - C_{gd}I_0L_DL_Gg_m + C_{iss}I_0L_DL_Gg_m - C_{gd}I_0L_DL_Sg_m + C_{iss}I_0L_DL_Sg_m - C_{gd}I_0L_GL_Sg_m + C_{iss}I_0L_GL_Sg_m + C_{gd}C_{oss2}L_2R_GV_0g_m + C_{gd}C_{oss2}I_0L_2R_GR_{loop}g_m - C_{iss}C_{oss2}I_0L_2R_GR_{loop}g_m)s^2 + (C_{oss}I_0L_D - C_{oss2}I_0L_2 - C_{gd}I_0L_S + C_{oss}I_0L_S + C_{gd}{}^2R_GV_0 - C_{iss}C_{oss}R_GV_0 + C_{gd}L_GV_0g_m - C_{oss2}I_0L_2R_{loop}g_m - C_{gd}I_0L_DR_Gg_m + C_{iss}I_0L_DR_Gg_m - C_{gd}I_0L_SR_Gg_m + C_{iss}I_0L_SR_Gg_m)s - C_{oss}V_0 + I_0L_Dg_m + C_{gd}R_GV_0g_m.$

REFERENCES

[1] N. Kaminski, "State of the art and the future of wide band-gap devices," in *Proc. 13th Eur. Conf. Power Electron. Appl.*, Sep. 2009, pp. 1–9.

[2] R. Ramachandran and M. Nymand, "Experimental demonstration of a 98.8% efficient isolated DC–DC GaN converter," *IEEE Trans. Ind. Electron.*, vol. 64, no. 11, pp. 9104–9113, Nov. 2017.

[3] J. Chen, Q. Luo, J. Huang, Q. He, and X. Du, "A complete switching analytical model of low-voltage eGaN HEMTs and its application in loss analysis," *IEEE Trans. Ind. Electron.*, vol. 67, no. 2, pp. 1615–1625, Feb. 2020.

[4] X. Huang, Q. Li, Z. Liu, and F. C. Lee, "Analytical loss model of high voltage GaN HEMT in cascode configuration," *IEEE Trans. Power Electron.*, vol. 29, no. 5, pp. 2208–2219, May 2014.

[5] K. Wang, X. Yang, H. Li, H. Ma, X. Zeng, and W. Chen, "An analytical switching process model of low-voltage eGaN HEMTs for loss calculation," *IEEE Trans. Power Electron.*, vol. 31, no. 1, pp. 635–647, Jan. 2016.

[6] T. Yao and R. Ayyanar, "A multifunctional double pulse tester for cascode GaN devices," *IEEE Trans. Ind. Electron.*, vol. 64, no. 11, pp. 9023–9031, Nov. 2017.

[7] X. Huang, W. Du, F. C. Lee, Q. Li, and W. Zhang, "Avoiding divergent oscillation of a cascode GaN device under high-current turn-off condition," *IEEE Trans. Power Electron.*, vol. 32, no. 1, pp. 593–601, Jan. 2017.

[8] Z. Zhang, B. Guo, and F. Wang, "Evaluation of switching loss contributed by parasitic ringing for fast switching wide band-gap devices," *IEEE Trans. Power Electron.*, vol. 34, no. 9, pp. 9082–9094, Sep. 2019.

[9] K. Wang, X. Yang, L. Wang, and P. Jain, "Instability analysis and oscillation suppression of enhancement-mode GaN devices in half-bridge circuits," *IEEE Trans. Power Electron.*, vol. 33, no. 2, pp. 1585–1596, Feb. 2018.

[10] Y. Li, M. Liang, J. Chen, T. Q. Zheng, and H. Guo, "A low gate turn-OFF impedance driver for suppressing crosstalk of SiC MOSFET based on different discrete packages," *IEEE J. Emerg. Sel. Topic. Power Electr.*, vol. 7, no. 1, pp. 353–365, Mar. 2019.

[11] J. Wang and H. S-H. Chung, "Impact of parasitic elements on the spurious triggering pulse in synchronous buck converter," *IEEE Trans. Power Electron.*, vol. 29, no. 12, pp. 6672–6685, Dec. 2014.

[12] R. Khanna, A. Amrhein, W. Stanchina, G. Reed, and Z.-H. Mao, "An analytical model for evaluating the influence of device parasitics on Cdv/dt induced false turn-on in SiC MOSFETs," in *Proc. 28th Annu. IEEE Appl. Power Electron. Conf. Expo.*, Long Beach, CA, USA, 2013, pp. 518–525.

[13] A. Lemmon, M. Mazzola, J. Gafford, and C. Parker, "Stability considerations for silicon carbide field-effect transistors," *IEEE Trans. Power Electron.*, vol. 28, no. 10, pp. 4453–4459, Oct. 2013.

[14] A. Lemmon, M. Mazzola, J. Gafford, and C. Parker, "Instability in half-bridge circuits switched with wide band-gap transistors," *IEEE Trans. Power Electron.*, vol. 29, no. 5, pp. 2380–2392, May 2014.

[15] Y. Sugihara *et al.*, "Analytical investigation on design instruction to avoid oscillatory false triggering of fast switching SiC-MOSFETs," in *Proc. IEEE Energy Convers. Congr. Expo.*, Cincinnati, OH, USA, 2017, pp. 5113–5118.

[16] P. Xue, L. Maresca, M. Riccio, G. Breglio, and A. Irace, "Self-sustained turn-off oscillation of SiC MOSFETs: Origin, instability analysis, and prevention," *Energies*, vol. 12, no. 11, 2019, Art. no. 2211.

[17] K. Saito, T. Miyoshi, D. Kawase, S. Hayakawa, T. Masuda, and Y. Sasajima, "Simplified model analysis of self-excited oscillation and its suppression in a high-voltage common package for Si-IGBT and SiC-MOS," *IEEE Trans. Electron Devices*, vol. 65, no. 3, pp. 1063–1071, Mar. 2018.
[18] W. Zhang, Z. Zhang, F. Wang, D. Costinett, L. Tolbert, and B. Blalock, "Common source inductance introduced self-turn-on in MOSFET turn-off transient," in *Proc. IEEE Appl. Power Electron. Conf. Expo.*, Tampa, FL, USA, 2017, pp. 837–842.
[19] P. Xue, L. Maresca, M. Riccio, G. Breglio, and A. Irace, "Analysis on the self-sustained oscillation of SiC MOSFET body diode," *IEEE Trans. Electron Devices*, vol. 66, no. 10, pp. 4287–4295, Oct. 2019.
[20] T. Yanagi, H. Otake, K. Nakahara, and T. Hikihara, "Self-sustained oscillation in half bridge circuit of silicon carbide devices with inductive load," in *Proc. Int. Symp. Nonlinear Theory Appl.*, 2015, pp. 876–879.
[21] K. Umetani, R. Matsumoto, and E. Hiraki, "Prevention of oscillatory false triggering of GaN-FETs by balancing gate-drain capacitance and common-source inductance," *IEEE Trans. Ind. Appl.*, vol. 55, no. 1, pp. 610–619, Jan./Feb. 2019.
[22] P. Xue, L. Maresca, M. Riccio, G. Breglio, and A. Irace, "Investigation on the self-sustained oscillation of superjunction MOSFET intrinsic diode," *IEEE Trans. Electron Devices*, vol. 66, no. 1, pp. 605–612, Jan. 2019.
[23] T. Liu, R. Ning, T. T. Y. Wong, and Z. J. Shen, "Modeling and analysis of SiC MOSFET switching oscillations," *IEEE J. Emerg. Sel. Topi. Power Electr.*, vol. 4, no. 3, pp. 747–756, Sep. 2016.
[24] I. Josifović, J. Popović-Gerber, and J. A. Ferreira, "Improving SiC JFET switching behavior under influence of circuit parasitics," *IEEE Trans. Power Electron.*, vol. 27, no. 8, pp. 3843–3854, Aug. 2012.
[25] M. Joko, A. Goto, M. Hasegawa, S. Miyahara, and H. Murakami, "Snubber circuit to suppress the voltage ringing for SiC device," in *Proc. PCIM Eur., Int. Exhib. Conf. Power Electron., Intell. Motion, Renewable Energy Energy Manage.*, Nuremberg, Germany, 2015, pp. 1–6.
[26] B. N. Torsæter, S. Tiwari, R. Lund, and O.-M. Midtgård, "Experimental evaluation of switching characteristics, switching losses and snubber design for a full SiC half-bridge power module," in *Proc. IEEE 7th Int. Symp. Power Electron. Distrib. Gener. Syst.*, 2016, pp. 1–8.
[27] R. A. Wood and T. E. Salem, "Evaluation of a 1200-V, 800-A all-SiC dual module," *IEEE Trans. Power Electron.*, vol. 26, no. 9, pp. 2504–2511, Sep. 2011.
[28] K. Yatsugi, K. Nomura, and Y. Hattori, "Analytical technique for designing an RC snubber circuit for ringing suppression in a phase-leg configuration," *IEEE Trans. Power Electron.*, vol. 33, no. 6, pp. 4736–4745, Jun. 2018.
[29] K. Harada and T. Ninomiya, "Optimum design of RC snubbers for switching regulators," *IEEE Trans. Aerosp. Electron. Syst.*, vol. AES-15, no. 2, pp. 209–218, Mar. 1979.
[30] J. Chen, Q. Luo, J. Huang, Q. He, P. Sun, and X. Du, "Analysis and design of an RC snubber circuit to suppress false triggering oscillation for GaN devices in half-bridge circuits," *IEEE Trans. Power Electron.*, vol. 35, no. 3, pp. 2690–2704, Mar. 2020.
[31] E. A. Jones, F. F. Wang, and D. Costinett, "Review of commercial GaN power devices and GaN-based converter design challenges," *IEEE J. Emerg. Sel. Topi. Power Electr.*, vol. 4, no. 3, pp. 707–719, Sep. 2016.
[32] A. Lidow, J. Strydom, M. de Rooij, J. Glaser, and D. Reusch, *GaN Transistors for Efficient Power Conversion*, 2nd ed. Hoboken, NJ, USA: Wiley, 2019.
[33] "Device models," GaN Systems, 2019. [Online]. Available: https://gansystems.com/gan-transistors/gs66508p/
[34] G. F. Franklin, J. D. Powell, and A. Emami-Naeini, *Feedback Control of Dynamic Systems*, 6th ed. Upper Saddle River, NJ, USA: Prentice-Hall, 2009.
[35] R. C. Dorf and R. H. Bishop, *Modern Control Systems*, 13th ed. Englewood Cliffs, NJ, USA: Pearson, 2016.

Jian Chen (Student Member, IEEE) was born in Hubei Province, China, in 1993. He received the B.S. degree in electrical engineering from Qinghai University, Xining, China, in 2016. He is currently working toward the Ph.D. degree in electrical engineering with Chongqing University, Chongqing, China.

His current research interests include wide bandgap device characteristics and models, active gate drivers, and power electronic integration.

Mr. Chen serves as a reviewer for some journals and conferences, such as the *IEEE Journal of Emerging and Selected Topics in Power Electronics* and the *IEEE ECCE-Asia*.

Quanming Luo (Member, IEEE) was born in Chongqing, China, in 1976. He received the B.S., M.S., and Ph.D. degrees in electrical engineering from Chongqing University, Chongqing, China, in 1999, 2002, and 2008, respectively.

From 2002 to 2005, he was a Research and Development Engineer with the Emerson Network Power Co., Ltd., Shenzhen, China. Since 2005, he has been with the College of Electrical Engineering, Chongqing University, where he is currently a Professor. He is the author or co-author of more than 80 papers in journal or conference proceedings. His current research interests include LED driving systems, communication power systems, power harmonic suppression, and power conversion systems in electrical vehicles.

Yuqi Wei (Student Member, IEEE) was born in Henan, China, in 1995. He received the B.S. degree from Yanshan University, Hebei, China, in 2016, and the M.S. degrees from the University of Wisconsin-Milwaukee, Milwaukee, WI, USA, in 2018, and Chongqing University, Chongqing, China, in 2019, respectively, all in electrical engineering. He is currently working toward the Ph.D. degree with the University of Arkansas, Fayetteville, AR, USA.

His current research interests include topology, modeling and control of dc/dc power converters and power factor correction ac/dc converters, wide bandgap devices, and active gate driving.

Mr. Wei serves as reviewer for the IEEE TRANSACTIONS ON INDUSTRIAL ELECTRONICS, the *IEEE Journal of Emerging and Selected Topics in Power Electronics*, the IEEE TRANSACTIONS ON INDUSTRY APPLICATIONS, the *IEEE Access*, and the *IET Power Electronics*.

Xinyue Zhang was born in Sichuan Province, China, in 1996. She received the B.S. degree in electrical engineering from the Harbin Institute of Technology, Weihai, China, in 2018. She is currently working toward the master's degree in electrical engineering with Chongqing University, Chongqing, China.

Her current research interests include the analytical modeling and the loss calculation of wide bandgap devices.

Xiong Du (Member, IEEE) received the B.S., M.S., and Ph.D. degrees from Chongqing University, Chongqing, China, in 2000, 2002, and 2005, respectively, all in electrical engineering.

Since 2002, he has been with Chongqing University, where he is currently a Full Professor with the School of Electrical Engineering. From 2007 to 2008, he was a Visiting Scholar with Rensselaer Polytechnic Institute, Troy, NY, USA. His research interest focuses on power electronics system reliability and stability.

Dr. Du was a recipient of the National Excellent Doctoral Dissertation of P.R. China, in 2008.